Title:

Sulfatide and neuronal complex gangliosides are functionally interdependent in maintaining myelinating axon integrity

Abbreviated title (50's): sulfatide & ganglioside interactions in the NS / membrane lipids determine CNS integrity / lipid interactions determine CNS integrity

Author names: McGonigal R[1], Barrie JA[1], Yao D[1], McLaughlin M[2], Cunningham ME[1], Rowan EG[3], Willison HJ[1]

Author affiliations: [1]University of Glasgow, Institute of Infection, Immunity & Inflammation G12 8TA; [2]University of Glasgow, School of Veterinary Biosciences G61 1QH ; [3] University of Strathclyde, Strathclyde Institute of Pharmacy & Biochemical Sciences G4 0RE

Corresponding author: Hugh J. Willison

Institute of Infection, Immunity & Inflammation

SGDB, B330

120 University Place, University of Glasgow

Glasgow G12 8TA

+44 0141 330 8388

Hugh.willison@glasgow.ac.uk

Number of pages: **36**

Number of figures, tables: 1 Table, 8 figures

Number of words: **1.** Abstract: 254

23 **2.** Introduction: 676

24 **3.** Discussion: 1617

25 **Conflict of Interest:** The authors declare no competing financial interests

26 **Acknowledgements:** **Wellcome, John Dempster

27

Abstract (250 words): reflects objectives and novelty. Include

- Objectives
- Methodology (include species studied and whether one or both sexes were included)
- Key Results
- Major Conclusion

Sulfatides and gangliosides are raft-associated glycolipids essential for maintaining myelinated nerve integrity. Mice deficient in sulfatide (cerebroside sulfotransferase knockout, *CST*$^{-/-}$) or complex gangliosides (β-1,4-N-acetylegalactosaminyltransferase 1 knockout, *GalNAc-T*$^{-/-}$) display prominent disorganization of protein localisation at the node of Ranvier (NoR) in early life, and age-dependent neurodegeneration. Loss of neuronal rather than glial complex gangliosides underpins the *GalNAc-T*$^{-/-}$ phenotype, as shown by neuron or glial-specific rescue whereas sulfatide is only expressed and functional in glial membranes. The similarities in NoR phenotype of *CST*$^{-/-}$, *GalNAc-T*$^{-/-}$ and axo-glial protein deficient mice suggests these glycolipids may stabilise membrane proteins including neurofascin 155 (NF155) and myelin-associated glycoprotein (MAG) at axo-glial junctions. To assess the functional interactions between sulfatide and gangliosides, *CST*$^{-/-}$ and *GalNAc-T*$^{-/-}$ genotypes were interbred. *CST*$^{-/-}$x *GalNAc-T*$^{-/-}$ mice develop normally to P10, but all die between P20-P25, coinciding with peak myelination. Ultrastructural, immunohistological and biochemical analysis reveals widespread axonal degeneration and disruption to the axo-glial junction at the NoR. In the CNS, in addition to sulfatide-dependent loss of NF155, *CST*$^{-/-}$*x GalNAc-T*$^{-/-}$ mice exhibited a major reduction in MAG protein levels in myelin, when compared to wild type and single lipid deficient mice. The *CST*$^{-/-}$x *GalNAc-T*$^{-/-}$ phenotype was fully restored to that of *CST*$^{-/-}$ mice by neuron-specific expression of complex gangliosides, but not by glial-specific expression, and not by the global expression of a-series gangliosides. These data indicate that sulfatide and complex b-series gangliosides on the glial and neuronal membranes respectively, act in concert to promote NF155 and MAG in maintaining the stable axo-glial interactions essential for normal nerve function.

Significance Statement (120 words max)

provide a clear explanation of the importance and relevance of the research in a manner accessible to researchers without specialized knowledge in the field and informed lay readers.

Sulfatides and complex gangliosides are membrane glycolipids with important roles in maintaining nervous system integrity. Node of Ranvier maintenance in particular requires stable compartmentalisation of multiple membrane proteins. The axo-glial adhesion molecules neurofascin 155 and myelin-associated glycoprotein require membrane microdomains containing either sulfatides or complex gangliosides to localise and function effectively. The co-operative roles of these microdomains and associated proteins are unknown. Here we show vital interdependent roles for sulfatides and complex gangliosides as double (but not single) deficiency causes a rapidly lethal phenotype in early age. These findings suggests that sulfatides and complex gangliosides on opposing axo-glial membranes are responsible for essential tethering of the axo-glial junction proteins, neurofascin155 and myelin-associated glycoprotein that interact to maintain the nodal complex. (120 words)

Introduction (650 words)

"briefly indicate the objectives of the study and provide enough background information to clarify why the study was undertaken and what hypotheses were tested"

Glycosphingolipids are highly enriched in lipid rafts (Simons and Toomre, 2000), involved in the topographical organisation of membrane proteins (Jackman et al., 2009; Sonnino et al., 2014; Sonnino et al., 2015). Sulfatide, 3-O-sulfogalactosylceramide, synthesised from galactocerebroside (GalC) by cerebroside sulfotransferase enzyme (**Figure 1A**) is enriched in the outer leaflet of the myelin membrane (Ishizuka, 1997). Complex ganglioside biosynthesis requires β-1,4-N-acetylegalactosaminyltransferase 1, *GalNAc-T* enzyme activity (**Figure 1A**) with ganglioside expression being widespread in both neuronal and glial membranes. Evidence indicates that both sulfatide and complex gangliosides are crucial for the maintenance and stability, rather than the developmental formation of nervous system domains (Takamiya et al., 1996; Honke et al., 2002). Mice deficient in these lipids thus develop relatively normally, before showing age-dependent degeneration[c1] (Takamiya et al., 1996; Honke et al., 2002). Evidence in particular indicates that these glycolipids are essential for stabilising the normal arrangement of axo-glial interactions, specifically at the paranodal region of the node of Ranvier (NoR). Mice deficient for GalC and sulfatide (Dupree et al., 1999), sulfatide alone (Ishibashi et al., 2002; Marcus et al., 2006; Hoshi et al., 2007) or complex gangliosides (Susuki et al., 2007) have prominently disrupted paranodes. The paranode in both the PNS and CNS tethers and seals the abutted axon and glial membranes between the node and juxtaparanode (Garcia-Fresco et al., 2006; Susuki et al., 2013), thereby maintaining nodal voltage-gated sodium (Nav) and juxtaparanodal potassium (Kv) channel clustering and segregation, essential for normal conduction (Salzer, 1997; Poliak and Peles, 2003). The importance of appropriate expression and localisation of the paranodal proteins in stabilising Nav channel clusters is also revealed in paranodal protein knockout mice. Thus deficiency in contactin, contactin-associated

protein (Caspr) or neurofascin (NF) 155 leads to progressive paranodal defects from P10 and subsequent axon degeneration, with most mice dying by P21 (Bhat et al., 2001; Boyle et al., 2001; Pillai et al., 2009). Significantly, while these adhesion complex proteins comprise the physical adhesion barrier at the paranode, associated glycolipid molecules appear to be required for their localisation and stabilisation, likely by the targeting and transportation of adhesion molecules in lipid rafts. In support of this Schafer et al. (2004), showed that sulfatide deficiency disrupted lipid rafts, leading to the loss of NF155 targeting to the paranode, thereby limiting its co-clustering function with axo-glial partners. Additionally, extraction studies identified sulfatide-containing lipid rafts as anchors for the axo-glial adhesion molecule myelin-associated glycoprotein (MAG), as well as NF155 (Pomicter et al., 2013).

Complex gangliosides are also an important lipid raft component required for paranode stabilisation, as shown by an absence of transverse bands and dissociation of paranodal proteins in *GalNAc-T*$^{-/-}$ mice (Susuki et al., 2007). As gangliosides are present in both neuronal and glial membranes, their principal site of action in paranodal stabilisation cannot be presumed. To address this, we demonstrated that loss of neuronal complex gangliosides underpins the *GalNAc-T*$^{-/-}$ phenotype as selective reintroduction of complex ganglioside expression in neuronal but not glial membranes rescues the paranodal phenotype (Yao et al., 2014). Complex gangliosides GT1b and GD1a, both prominently expressed on the axonal membrane, are *trans* receptors for glial membrane-associated MAG (indicated in **Figure 1A**)(Collins et al., 1997; Vinson et al., 2001). Analysis of protein extracts demonstrated a reduction in MAG levels in *GalNAc-T*$^{-/-}$ mice (Sheikh et al., 1999; Kawai et al., 2001), which suggests that complex neuronal gangliosides and glial MAG cooperatively contribute to the stability of the axo-glial junction.

Importantly, loss of sulfatide does not alter ganglioside content (Honke et al., 2002) and complex ganglioside deficiency does not alter sulfatide content (Yamashita et al., 2005) which suggests their expression is not directly inter-linked in a compensatory way, but nevertheless might be additive

functionally. Herein we considered that as these glycolipids are differentially expressed in glial and axonal membranes, they may act in partnership to retain clustered proteins in their respective domains. We sought to test this by interbreeding strains of single null mice and neuronal and glial specific rescue mice, thereby allowing us to assess interdependency and cooperativity in the role of axonal and glial glycolipids in paranodal organisation.

Methods

- Give sufficient detail to permit repetition of the work by others:
- Reference should be made to published procedures wherever possible; this applies to the original description and pertinent published modifications.
- The sex of subjects should be stated
- All companies from which materials were obtained should be listed. *RRIDS*
- If materials were obtained from an individual, an affiliation for that individual should be listed.
- *Neurosci* requires every research manuscript to include an Experimental Design and Statistical Analysis section as a subsection of the Materials and Methods that describes the experimental design and the statistical tests used in the study

Mice. Seven mouse lines on the C57Bl/6 background were used and generated: 1. Wild type (WT); 2. *GalNAc-T$^{-/-}$;* 3. *CST$^{-/-}$;* 4. *CST$^{-/-}$ x GalNAc-T$^{-/-}$-Tg(neuronal);* 5. *CST$^{-/-}$ x GD3s$^{-/-}$;* 6. *CST$^{-/-}$ x GalNAc-T$^{-/-}$*; 7. *CST$^{-/-}$ x GalNAc-T$^{-/-}$-Tg(glial);* (group number and age are described per experiment below). Generation of *GalNAc-T$^{-/-}$* and *CST$^{-/-}$* transgenic mice has previously been described (Takamiya et al., 1996; Honke et al., 2002) and were interbred to produce the *CST$^{-/-}$ x GalNAc-T$^{-/-}$* genotype. Double null mice with reconstituted site-specific expression of complex gangliosides were produced by crossing the *CST$^{-/-}$* genotype with previously described *GalNAc-T$^{-/-}$-Tg(neuronal)* or *GalNAc-T$^{-/-}$-Tg(glial)* strains (Yao et al., 2014) or *GD3s$^{-/-}$* (Okada et al., 2002) resulting in *CST$^{-/-}$ x GalNAc-T$^{-/-}$-Tg(neuronal)*, *CST$^{-/-}$ x GalNAc-T$^{-/-}$-Tg(glial)* and *CST$^{-/-}$ x GD3s$^{-/-}$*, respectively. *CST$^{-/-}$ x GalNAc-T$^{-/-}$-Tg(glial)* bred poorly and there were insufficient numbers to fully phenotype; therefore their inclusion was restricted to survival data and phenotypic analysis. Mice were maintained under a 12 hour light/dark cycle in controlled temperature and humidity with unlimited access to food and water. For each study, m~~M~~ice of either sex [m2]were killed by rising CO_2 inhalation; all experiments using mice were performed in accordance with a licence approved and granted by the United Kingdom Home Office and conformed to University of Glasgow institutional guidelines. Experiments complied

with relevant guidelines on the care and use of animals outlined in the revised Animals (Scientific Procedures) Act 1986.

Phenotypic analysis of mice. Weights were obtained at P22 from wild type (n=5), *GalNAc-T*$^{-/-}$ (n=5), *CST*$^{-/-}$ (n=4), *CST*$^{-/-}$ *x GalNAc-T*$^{-/-}$*-Tg(neuronal)* (n=4), *CST*$^{-/-}$ *x GD3s*$^{-/-}$ (n=6) and *CST*$^{-/-}$ *x GalNAc-T*$^{-/-}$ (n=10) mice. Data points from every animal per genotype were plotted, and the mean and S.E.M displayed. Survival plots for all genotypes were plotted over 200 days for each genotype: wild type (n=7); *GalNAc-T*$^{-/-}$ (n=10); *CST*$^{-/-}$ (n=18); *CST*$^{-/-}$ *x GalNAc-T*$^{-/-}$*-Tg(neuronal)* (n=6); *CST*$^{-/-}$ *x GD3s*$^{-/-}$ (n=38), *CST*$^{-/-}$ *x GalNAc-T*$^{-/-}$*-Tg(glial)* mice (n=12); and *CST*$^{-/-}$ *x GalNAc-T*$^{-/-}$ (n=29). Mice were photographed when suspended by the tail to record hind-limb leg splaying (a feature of many neurodegenerative mutants), and gross brain anatomy was also recorded upon brain removal at P22.

Materials. Monoclonal antibodies used to detect complex a- or b-series gangliosides by immunofluorescent staining were generated and described previously (Bowes et al., 2002; Boffey et al., 2005). Anti-GM1 ganglioside antibody, DG2, and anti-GD1b antibody, MOG1, were used at 20 µg/ml. A new monoclonal anti-sulfatide antibody, GAMEG3, derived from mice inoculated with sulfatide-bearing liposomes was used to detect sulfatide (Meehan et al., in press). Primary antibodies were used as follows: mouse anti-phosphorylated neurofilament-H antibody (NF-H, BioLegend; RRID:AB_2715851; 1:2000); rat anti-MBP (BioRad; RRID:AB_325004; 1:500); mouse anti-pan Nav (Sigma; RRID:AB_477552; 1:100); mouse anti-ankyrin G (ThermoFisher scientific; RRID:AB_2533145; 1:100); rabbit anti-Caspr (gifted from Professor Peles, Weizmann Institute, Israel; 1:1500); rabbit anti-Kv1.1 (Alomone labs; RRID:AB_2040144; 1:200); rabbit anti-Nav1.6 (Sigma; RRID:AB_477480; 1:100); rabbit anti-pan neurofascin (gifted from Professor Brophy, University of Edinburgh, UK; pNFasc 1:1000); mouse anti-MAG antibody (gifted from Professor Brophy, University of Edinburgh, UK; 1:100). Primary antibodies used in Western blots were rabbit anti-MAG 248 (gifted from Prof. N Groome, 1:10000[m3])(Barrie et al., 2010) and rabbit anti-NF155 (gifted from Professor

Brophy, University of Edinburgh, UK; 1:5000) were prepared in 5% semi-skimmed milk in TBS containing 0.1% Tween-20 (T-TBS). Secondary antibodies were made in PBS plus 1% NGS: isotype-specific (IgG1, IgG3) Alexa Fluor 488- and 555-conjugated goat anti-mouse IgG antibodies (Molecular Probes; RRID:AB_141780); Alexa Fluor 488- and 555-conjugated goat anti-rabbit (Molecular Probes; RRID:AB_141761) and anti-rat IgG antibodies (Molecular Probes; RRID:AB_141733). Secondary antibody for western blots was HRP-linked goat anti-rabbit (Dako, 1:10 000) prepared in 5% skimmed milk/T-TBS.

Immunostaining , Image acquisition and analysis.

Lipid localisation: Snap-frozen peripheral nerves were transversely sectioned at 10µm and collected onto APES-coated slides (n=3/genotype). Sections were treated with 100% EtOH for 10 min at -20°C then thoroughly washed in PBS. Antibodies were applied to the sections overnight at 4°C in the following combinations: 1) anti-ganglioside antibody DG2 or MOG1 with anti-phosphorylated NF-H antibody; 2) anti-sulfatide antibody with anti-MBP antibody. Sections were PBS washed secondary antibodies applied for 1h at R.T. Slides PBS washed and mounted in citifluor. Representative images were captured at 40x magnification using a Zeiss AxioImager Z1 with ApoTome attachment and processed using Zeiss Zen 2 blue edition software.

Nodal protein immunostaining: Sciatic nerves (SN) and optic nerves (OpN) were fixed for 30 min in 4% PFA upon removal from P22 mice (n=3/4 per genotype). Subsequently nerves were cryoprotected in 30% sucrose, and either gently teased into single fibres (SN) collected on slides, or frozen in OCT mounting medium and longitudinally sectioned at 10 µm (OpN). To study nodal protein localization, teased SN were immunostained with primary antibodies for either anti- Nav1.6, anti-Kv1.1 or pNFasc, and OpN sections were immunostained with primary antibodies for combinations of anti- pNav and anti-pNFasc, or anti-Caspr and anti-AnkG. OpN sections and unfixed peripheral nerve sections were stained with anti- MAG antibody. Nerves were pre-treated with blocking solution (10% normal goat serum + 0.3% Triton X-100) for 1 h at 4°C before incubation

overnight in the same solution plus primary antibody combinations at the same temperature. Triton was omitted from blocking and incubation solutions when using unfixed peripheral nerve sections. Samples were washed 3x 5 min then incubated for 2 h at room temperature in secondary antibody solution. Slides were coverslipped [c4]in citifluor mount medium after three further 5 min PBS washes. All nodal protein images were captured at 63x magnification, and MAG immunostained tissue at 40x magnification using a Zeiss AxioImager Z1 with ApoTome attachment and processed with Zeiss Zen 2 blue edition software. For teased sciatic nerves, 20 NoR on average were imaged and quantified per mouse for each stain. For optic nerve double-staining combinations, three 10 µm thick z-stacks (30 slices, step value 0.34 µm) were captured per mouse. Four 50 x 50 µm fields of view (FOV) per stack were analysed for either pNav channel cluster number, number of Nav channel clusters flanked by intact NFasc dimers, or intact Caspr dimers, using NIH ImageJ software (RRID:SCR_003070). Clusters/dimers were included in the count if they overlaid the top and right-side borders of the FOV, and excluded when they overlaid the left-side or lower borders. For MAG staining intensity analysis, single slices were captured at set exposures from 3 slides per genotype. Graphs ± S.E.M or box-and-whisker plots were used to display the spread of all data points collected from each animal then means were calculated per genotype for statistical analysis.

Ultrastructure. Mice (WT n=5, *GalNAc-T*$^{-/-}$ n=6, *CST*$^{-/-}$ n=6, *CST*$^{-/-}$ *x GalNAc-T*$^{-/-}$*-Tg(neuronal)* n=6, *CST*$^{-/-}$ *x GD3s*$^{-/-}$n=6, *CST*$^{-/-}$ *x GalNAc-T*$^{-/-}$ n=5) were transcardially perfused at P25 with 5% glutaraldehyde/4% paraformaldehyde mixture before the optic nerve was removed and processed for resin embedding, as previously described (Griffiths et al., 1981). Sections were cut for both light and ultrastructural analysis. Electron micrographs from transverse sections of the optic nerve at 6700x magnification, were captured on a Jeol CX-100 Electron microscope. For quantification, a minimum of 10 electron micrographs per animal were taken of randomly selected fields. All measurements were made on scanned images using NIH ImageJ software. For axon morphometry and quantification of axonal changes, all axons within or touching the top and left borders of an area

of interest (AOI) were counted. The axon density and number of degenerating axons within the AOI were counted. Averaged values from every animal per genotype was plotted, and the mean and S.E.M displayed.

Extracellular recordings.

Perineural recordings were made from triangularis sterni nerve-muscle preparations set up as previously described (Braga et al., 1991; McGonigal et al., 2010). Recordings were made from small nerve bundles from each genotype (WT n=5, *GalNAc-T*$^{-/-}$ n=2, *CST*$^{-/-}$ n=3, *CST*$^{-/-}$ *x GalNAc-T*$^{-/-}$ n=2). Perineural Nav and Kv channel waveforms were collected during a paired pulse stimulation protocol. A representative graph plotting the peak Nav and Kv values as a percentage of the baseline waveforms at each interstimulus interval (ISI) was used to convey recovery of the nodal ion channel currents. A two-way ANOVA was used to compare the difference between genotypes, and post-hoc multiple comparisons to measure differences at each ISI.

Conduction velocity was measured in sciatic nerve (WT n=3, *GalNAc-T*$^{-/-}$ n=4, *CST*$^{-/-}$ n=4, *CST*$^{-/-}$ *x GalNAc-T*$^{-/-}$ n=5), as previously described (McGonigal et al., 2010). Optic nerves (between the eyeball and the optic chiasm) were quickly removed into oxygenated (95% O_2 and 5% CO_2) physiological Ringer's solution containing (mM): NaCl, 129; KCl, 3; NaH2PO4, 1.2; CaCl2, 2.4; MgSO4, 1.3; HEPES, 3; NaHCO3, 20; and glucose, 10. The nerves were mounted in a recording chamber and each end drawn into suction electrodes for electrophysiological studies (WT n=4, *GalNAc-T*$^{-/-}$ n=4, *CST*$^{-/-}$ n=4, *CST*$^{-/-}$ *x GalNAc-T*$^{-/-}$*-Tg(neuronal)* n=3, *CST*$^{-/-}$ *x GD3s*$^{-/-}$n=6, *CST*$^{-/-}$ *x GalNAc-T*$^{-/-}$ n=3). Compound action potentials were evoked by a supramaximal stimulus (Grass S88 stimulator), applied via a suction electrode at the proximal cut end, and recorded from a second suction electrode at the distal cut end. Signals were amplified (CED1902), digitized (NIDAQ-MX A/D converter, National Instruments, Austin, TX, USA) and analysed using WinWCP version 4.1.0 (J. Dempster, Strathclyde University, RRID:SCR_014713). Nerves were crushed ~~to confirm the waveforms were real~~ at the end of the experiment in order to identify and exclude electrical artefacts from the analysis. Nerve conduction

velocity was calculated by dividing the length of the nerve by latency (the time between the stimulation artefact and the highest peak of compound action potential). Average values from every animal per genotype were plotted, and the mean and S.E.M displayed.

Western blot. Mouse brains were removed (n=4/genotype), snap frozen in liquid nitrogen, and stored at -80°C until required. Myelin preparation was conducted using a modification of the method by Norton and Poduslo (1973). Briefly, brains were homogenised in a buffer composed of 0.85 M sucrose, 10 mM Hepes, pH 7.4, 2 mM DTT, and 1 mM TLCK for 20 sec using an Ultra-Turrax T8 blender (IKA-Works Inc., Wilmington, NC) set at maximum speed and 0.25 M sucrose gently layered on top of the homogenate and then centrifuged at 70,000g for 90 min at 4°C. The myelin interface was collected, hypotonically lysed in chilled dH2O and pelleted at 23,000g for 30 min at 4°C. Following an additional two rounds of hypotonic lysis, the myelin pellet was resuspended in 10 mM Hepes, pH 7.4, containing 1x protease inhibitor cocktail (Sigma). The myelin fraction was stored at -80°C until required. The protein concentration was determined using a bicinchoninic acid method employing BSA as a standard (Pierce, Thermo Scientific). SDS-PAGE/ Western blot analysis was conducted as previously described (Yool et al., 2001). In brief, 1 and 5 ug of myelin was denatured in Laemmli buffer, separated on a 4-12% gel (Biorad), and transferred to nitrocellulose membrane (Invitrogen). The membrane was blocked with 5% skimmed milk in TBS containing 0.1% Tween-20 (T-TBS) for 1hr at room temperature, then incubated in primary antibodies overnight at 4°C on an orbital shaker. Following three 10 min washes in T-TBS, the immunocomplex was detected with the HRP-linked secondary antibody (Dako) and visualised using the ECL reaction as per manufacturer's instructions (Pierce, Thermo Scientific). Densitometric analysis of the Western blots was performed using Image J software (NIH). Average values from every animal per genotype were plotted, and the mean and S.E.M displayed.

Experimental design and statistical analysis. The number of independent animals are described in the Methods and Results sections and indicated in figure legends. Statistical differences among genotypes were determined by one-way or two-way ANOVA followed by a Fisher's or Tukey's *post-hoc* tests using GraphPad Prism 6 software (RRID:SCR_002798). Differences were considered significant when~~at~~ $p < 0.05$.

Results

- present the experimental findings, clearly and succinctly. Only results essential to establish the main points of the work should be included. Experimental conclusions should normally be based on an adequate number of observations with statistical analysis of variance and the significance of differences.

- Authors must provide detailed information for each statistical test applied including: the type of test; specific p values (not > or <); degrees of freedom; population size; definition of population (e.g., number of individual measurements, number of animals of each sex, number of slices, number of times treatment was applied, etc.); and if performed, what correction was used to adjust for multiple pairwise comparisons
- *JNeurosci* requires every research manuscript to report in full the complete results of the statistical analyses, including degrees of freedom and any estimates of effects size, should be reported in the Results section. Report exact p values rather than ranges (e.g. p = 0.026 rather than p < 0.05). There are many types of analyses that can be reported, but examples include F values (F(1, 72) = 14.5, p = 0.003, ANOVA), t values (t(10) = 2.98, p = 0.043, paired t-test)

Ganglioside and sulfatide expression is successfully eliminated in CST$^{-/-}$ x GalNAc-T$^{-/-}$ mice

To investigate the interaction between ganglioside and sulfatide lipids on nervous system integrity, we studied six transgenic mouse lines: wild type; *GalNAc-T$^{-/-}$*; *CST$^{-/-}$*; *CST$^{-/-}$ x GalNAc-T$^{-/-}$-Tg(neuronal);* *CST$^{-/-}$ x GD3s$^{-/-}$*; and *CST$^{-/-}$ x GalNAc-T$^{-/-}$*. **Table 1** provides an overview of the specific glycolipid expression and deficiency profiles among the mice generated for this study. We confirmed the presence of targeted gene disruption and reintroduction in these transgenic lines by PCR and screening for complex ganglioside or sulfatide expression in neural tissue by immunostaining

(**FIGURE 1**). An additional line, *CST$^{-/-}$ x GalNAc-T$^{-/-}$-Tg(glial)* was subsequently generated for comparative survival plots.

The CST, GalNAc-T and GD3s genes are disrupted by an insert, which was assessed by PCR. From the gels in **Figure 1B**, the larger band represents successful GalNAc-T gene disruption in *GalNAc-T$^{-/-}$*, *CST$^{-/-}$ x GalNAc-T$^{-/-}$-Tg(neuronal)* mice and *CST$^{-/-}$ x GalNAc-T$^{-/-}$* mice, and CST disruption in *CST$^{-/-}$*, *CST$^{-/-}$ x GalNAc-T$^{-/-}$-Tg(neuronal)* mice, *CST$^{-/-}$ x GD3s$^{-/-}$* and *CST$^{-/-}$ x GalNAc-T$^{-/-}$* mice. The smaller band confirms GD3 synthase (GD3s) gene disruption in *CST$^{-/-}$ x GD3s$^{-/-}$* mice. Additionally, a band identifying the GalNAc-T-flag [m5]in the *CST$^{-/-}$ x GalNAc-T$^{-/-}$-Tg(neuronal)* mouse strain confirms selective GalNAc-T gene re-expression neuronally.

Confirmation of ~~A~~absence or selective expression of lipids was assessed in all genotypes ~~by staining peripheral[m6] nerves~~ with two anti-ganglioside antibodies that detected either the a- or b-series complex gangliosides, and an anti-sulfatide antibody. Qualitative results for immunostaining with these antibodies in the peripheral nerve are shown in ~~(~~**FIGURE 1C**~~)~~. As expected, neural tissue from all genotypes except *GalNAc-T$^{-/-}$* mice and *CST$^{-/-}$ x GalNAc-T$^{-/-}$* mice was positive for anti-GM1 (a-series) antibody immunolabeling. Additionally, anti-GD1b antibody (b-series) binding was undetectable in the latter two genotypes confirming absence of all a- and b-series gangliosides. Similarly, nerves from *CST$^{-/-}$ x GD3s$^{-/-}$* mice, null for b-series ganglioside expression, had no observable immunolabeling with the anti-GD1b antibody. Both a- and b-series gangliosides were successfully reintroduced in the axons of the *CST$^{-/-}$ x GalNAc-T$^{-/-}$-Tg(neuronal)* mouse line as shown by positive anti-GM1 and anti-GD1b immunoreactivity. When neural tissue was immunostained with anti-sulfatide antibody, positively labelled myelin was observed in wild type and *GalNAc-T$^{-/-}$* mice nerves, while no labelling was detected in the other four genotypes, confirming the absence of sulfatide expression with CST gene knock out.

Ganglioside and sulfatide double null mice have a significantly reduced lifespan

The complex ganglioside null and sulfatide null mouse strains have an age-dependent degenerative phenotype that manifest clinically from 4 months and 6 weeks respectively. In contrast to each of the single glycolipid deficient mice, the *CST*$^{-/-}$ *x GalNAc-T*$^{-/-}$ mice exhibited a very severe phenotype from 2 weeks, lethal by 4 weeks. The mouse appears to develop normally and is similar in size to wild type and single knock out mice, then subsequently fails to thrive, declining in body weight beyond P15 and showing a significant reduction in weight at P22 (one-way ANOVA $F(5,28) = 18.15$, $p<0.0001$[c7])(**FIGURE 2A**[m8]). Single pup rearing through removal of litter-mates on three occasions did not prolong survival. *CST*$^{-/-}$ *x GalNAc-T*$^{-/-}$ mice exhibit a hunched, emaciated appearance, develop a tremor and display hind-limb leg splaying (**FIGURE 2B)**, a typical characteristic of the single knock out mice at later stages of life. Despite reduction in weight, macroscopic brain (**FIGURE 2B)** and nerve ~~trunk~~ anatomy[m9][RM10] appear normal.

Survival plots demonstrate that incrementally diminishing ganglioside and sulfatide expression corresponds with a reduction in life expectancy, measured up to 200 days (**FIGURE 2C**).Wild type and *GalNAc-T*$^{-/-}$ mice have a normal life expectancy up to 200 days. *CST*$^{-/-}$ *x GalNAc-T*$^{-/-}$ mice have the shortest life expectancy of the lines studied, never surviving beyond 4 weeks, with the majority only surviving to P21-P25. In the absence of sulfatide expression, but with normal ganglioside expression, *CST*$^{-/-}$ life expectancy at 200 days more than halves. In mice lacking sulfatide and complex gangliosides globally but with all complex gangliosides reintroduced specifically into neurons (i.e. the *CST*$^{-/-}$ *x GalNAc-T*$^{-/-}$*-Tg(neuronal)* mouse), life expectancy is restored to that of sulfatide null mice, with 60% of mice surviving to at least 200 days. Additionally, weight at P22 is comparable in this genotype to WT, *CST*$^{-/-}$ and *GalNAc-T*$^{-/-}$ mice (**FIGURE 2A**). In order to determine whether a- or b-series complex ganglioside deficiency was responsible for the severity of the double sulfatide and complex ganglioside null mouse, we examined mice that expressed a-series gangliosides only and lacked b-series gangliosides (achieved through crossing sulfatide and b-series null mice). These were only modestly improved relative to the *CST*$^{-/-}$ *x GalNAc-T*$^{-/-}$ phenotype, as shown by the failure to thrive and significant weight loss at P22. Life expectancy is severely reduced with only 50% survival

at 4 weeks, and less than 10% mice reaching a maximum of 21 weeks. To determine the importance of neuronal relative to glial ganglioside expression, *CST$^{-/-}$ x GalNAc-T$^{-/-}$* mice were generated with glial expression of complex gangliosides, i.e. *CST$^{-/-}$ x GalNAc-T$^{-/-}$-Tg(glial)*. Unlike the successful rescue of the lethal phenotype with neuronal complex gangliosides, expression of compelx gangliosides in glial membranes did not improve *CST$^{-/-}$ x GalNAc-T$^{-/-}$* survival. Therefore based on survival data, the genotypes can be categorised into three subsets: mild (WT, *GalNAc-T$^{-/-}$*); moderate (*CST$^{-/-}$*, *CST$^{-/-}$ x GalNAc-T$^{-/-}$-Tg(neuronal)*; and severe (*CST$^{-/-}$ x GD3s$^{-/-}$*, *CST$^{-/-}$ x GalNAc-T$^{-/-}$*).

Loss of both sulfatide and complex gangliosides results in a disruption to CNS nodes of Ranvier

Age-dependent loss of nodal integrity is evident in both single ganglioside and sulfatide null mice and could potentially contribute to loss of normal ion channel clustering, functional deficits and axon degeneration. Of the single lipid deficient mice, disrupted nodal integrity is more rapid and pronounced in the sulfatide null mice, beginning post-myelin development (>1 month). To assess whether this process was enhanced or accelerated in *CST$^{-/-}$ x GalNAc-T$^{-/-}$* mice, we initially assessed changes in both the PNS [m11](sciatic nerve, internal intercostal nerve) and the CNS (optic nerve, brain) at P22. When the PNS integrity was examined, ~~We~~ we found that combined sulfatide and complex ganglioside deficiency did not augment the disorganisation of proteins at the node of Ranvier ~~in the PNS~~ of the single sulfatide null mice (**Figure 3A**). Peripheral nerve Nav channel clusters were lengthened both in *CST$^{-/-}$* and *CST$^{-/-}$ x GalNAc-T$^{-/-}$* sciatic nerves. Despite ANOVA reaching significance, post-hoc multiple comparisons showed the Nav channel cluster lengths in the latter genotypes did not reach significance compared to WT, *GalNAc-T$^{-/-}$* or each other (one-way ANOVA, $F(3,9)=.5794$, $p=0.0491$). In both *CST$^{-/-}$* and *CST$^{-/-}$ x GalNAc-T$^{-/-}$* sciatic nerve nodes of Ranvier immunostaining for Kv1.1 channel domains, normally located at the juxtaparanodes, invaded the paranodal region, shown by a shortening in the distance between the staining domains, compared to WT and *GalNAc-T$^{-/-}$* nerves (one-way ANOVA, $F(3,9)$, $p<0.0001$). pNFasc staining did not significantly change between

genotypes (one-way ANOVA, F(3,9) = 1.157, p= 0.38) suggesting no impairment of NF155 paranodal clustering in peripheral nerve at P22. Additionally, electrophysiological function did not significantly worsen in *CST*$^{-/-}$ *x GalNAc-T*$^{-/-}$ peripheral nerve compared to single sulfatide deficient nerve based on paired pulse stimulations and conduction velocity measurements (**Figure** [c12]**3B**). We performed perineural recordings to assess the Nav and Kv channel currents of the internal intercostal nerve that innervates the TS muscle. The recovery of both peaks after paired pulse stimulation was significantly different among genotypes (Nav peak: two-way ANOVA, F(3,117) = 10.79, p<0.0001. Kv peak: two-way ANOVA, F(3,117) = 32.24, p<0.0001). Both *CST*$^{-/-}$ and *CST*$^{-/-}$ *x GalNAc-T*$^{-/-}$ peaks were significantly reduced in the initial interstimulus intervals compared to WT and *GalNAc-T*$^{-/-}$ preparations, as indicated on the graphs in **Figure 3B**. Conduction velocity was slower in *GalNAc-T*$^{-/-}$, *CST*$^{-/-}$ and *CST*$^{-/-}$ *x GalNAc-T*$^{-/-}$ sciatic nerve compared to *WT*, but only reached significance in *CST*$^{-/-}$ nerve (one-way ANOVA, F(3,12) = 3.939, p = 0.036). MAG immunostaining was comparable in peripheral nerves of all four genotypes (**Figure 3C**). It is thus unlikely that PNS dysfunction and degeneration would account for the lethal phenotype in double deficient mice and there was no evidence of further disruption to the PNS in the double deficient mice compared to the sufatide null mice. As such, we then focussed our attention on the CNS with additional Tg lines.

When comparing Nav channel clustering in the optic nerve from all genotypes there is a significant reduction in Nav channel cluster number (one-way ANOVA (F(5,13) = 4.76, p=0.0108). *CST*$^{-/-}$ *x GalNAc-T*$^{-/-}$ mice have fewer Nav channel clusters than all other genotypes, but this reduction only reached significance when compared to wild type and complex ganglioside deficient mice, which were not significantly different to each other (**FIGURE 4A**). Although reduced, the number of Nav channel clusters is within the normal wild type range when sulfatide is expressed or complex gangliosides are reintroduced in the neuronal membrane in *CST*$^{-/-}$ *x GalNAc-T*$^{-/-}$*-Tg(neuronal)* mice. This is not the case when a-series gangliosides are expressed globally on the sulfatide null background in *CST*$^{-/-}$ *x GD3s*$^{-/-}$ mice, which have similar cluster numbers to *CST*$^{-/-}$ *x GalNAc-T*$^{-/-}$ mice. Since cluster number does not explicitly define mature nodes of Ranvier, the number of Nav channel

clusters flanked laterally by intact paranodal neurofascin dimers were assessed. Earlier reports have shown that lack of sulfatide attenuates neurofascin 155 localisation to the paranodal region (Ishibashi et al., 2002; Schafer et al., 2004; Marcus et al., 2006), and indeed we found all four lines with sulfatide deficiency had significantly fewer neurofascin positive paranodal dimers flanking Nav channel clusters as early as P22 compared to wild type and *GalNAc-T*$^{-/-}$ mice (one-way ANOVA ($F_{5,13}$) = 21.31, $p<0.0001$)(**FIGURE 4B,C**). A pan-neurofascin antibody was used that detects both the neuronal NF186 and glial NF155 isoforms critical for Nav channel clustering and paranodal axo-glial junction formation, respectively. We detected no change to NF186 [m13][RM14]presence and observed normal co-localisation with Nav channel clusters suggesting this isoform is not impacted by ganglioside or sulfatide lipid expression.

Further analysis showed paranodal Caspr dimers were significantly reduced at P22 in all genotypes, with the exception of *GalNAc-T*$^{-/-}$ mice, compared to wild type mice (one-way ANOVA ($F_{5,14}$) = 8.8, $p=0.0006$) (**FIGURE 5**). However, significance was greatest when wild type was compared to *GalNAc-T*$^{-/-}$ *x CST*$^{-/-}$ and *CST*$^{-/-}$ x *GD3s*$^{-/-}$ mice. *GalNAc-T*$^{-/-}$ *x CST*$^{-/-}$ mice also showed a significant reduction compared to *CST*$^{-/-}$ and *CST*$^{-/-}$ *x GalNAc-T*$^{-/-}$*-Tg(neuronal)* nerves. Expression of neuronal a- and b-series gangliosides improved the feature under examination, but global a-series ganglioside expression did not.

Glycolipid deficiency reduces CNS axon integrity and function

Age-dependent degeneration beyond 2 months of age is a feature of the *CST*$^{-/-}$ and the *GalNAc-T*$^{-/-}$ mouse strains. The principal ultrastructural abnormality observed in the current study was early onset CNS axon degeneration in the *CST*$^{-/-}$ *x GalNAc-T*$^{-/-}$ mice. There was a significant increase in degenerating axons in the optic nerve at P25 with diminishing glycolipid expression (one-way ANOVA ($F_{5,27}$) = 11.51, $p<0.0001$). *CST*$^{-/-}$ *x GalNAc-T*$^{-/-}$ mice had significantly more degenerate axons compared to wild type and *GalNAc-T*$^{-/-}$ nerves, which are comparable (**FIGURE 6A**). The

number of degenerate axons in *CST*$^{-/-}$ mice was very variable and reached significance, albeit a lower level compared to wild type. Additionally, the number of degenerate axons were fewer than observed for *CST*$^{-/-}$ *x GalNAc-T*$^{-/-}$ optic nerve but this difference did not reach significance. A protection of axons from degeneration was achieved by reinstatement of both a- and b-series gangliosides neuronally, leading to a reduction in the number of degenerate axons to within wild type levels. However, the number of degenerate axons was not improved by expression of global a-series ganglioside expression in the *CST*$^{-/-}$ *x GD3s*$^{-/-}$ strain, which were equal to *CST*$^{-/-}$ *x GalNAc-T*$^{-/-}$ levels. Electron micrographs show the normal formation of myelin in large diameter myelinated ~~fibres~~ fibres, alongside abundant unmyelinated and thinly myelinated fibres undergoing myelin maturation in all genotypes (**FIGURE 6B**). ~~As peak myelination is in progress at the time-point studied, abundant unmyelinated fibres and thin myelin was observed in all genotypes in the electron micrographs, making it uninformative to undertake a meaningful analysis of myelin formation or maintenance[m15][RM16].~~

To investigate the functional consequence of degenerating axons and nodal structure disturbance, conduction velocity was recorded from isolated optic nerve at P22 (**FIGURE 6C**). Conduction velocity was significantly reduced with diminishing glycolipid expression (one-way ANOVA ($F(5,18) = 4.25$, $p<0.01$), which correlated with the survival plots, nodal and ultrastructural data. The~~re was a significant~~ reduction in CV did not reach significance between any of the genotypes in post-hoc analysis. The waveforms ~~became~~were abnormal [c17]in *CST*$^{-/-}$, *CST*$^{-/-}$ *x GD3s*$^{-/-}$ and *CST*$^{-/-}$ *x GalNAc-T*$^{-/-}$ optic nerves as compared to wild type, ~~and *GalNAc T*$^{-/-}$ mouse nerves. *CST*$^{-/-}$ *x GalNAc T*$^{-/-}$ conduction velocity was reduced compared to *CST*$^{-/-}$ but this did not reach significance~~with broader waveforms that followed a different peak formation. ~~Once more, t~~There was an ~~modest~~ improvement in *CST*$^{-/-}$ *x GalNAc-T*$^{-/-}$*-Tg(neuronal)* ~~with optic nerve conduction velocity rates reaching~~waveform ~~within the~~to normal wild type ~~and *GalNAc-T*$^{-/-}$ range and significantly greater than those rates recorded from *CST*$^{-/-}$ *x GD3s*$^{-/-}$ and *CST*$^{-/-}$ *x GalNAc-T*$^{-/-}$ optic nerve. Although increased, the difference in *CST*$^{-/-}$ *x GalNAc-T*$^{-/-}$*-Tg(neuronal)* conduction velocity compared to CST$^{-/-}$ mice did not reach significance~~ appearance.[c18]

MAG protein expression in myelin is disrupted in sulfatide and ganglioside double null mice

Sulfatide deficiency has previously been reported to alter expression of key myelin proteins, prompting us to interrogate the differences in the expression of these proteins in the 6 genotypes studied. Expression of the major myelin proteins PLP and MBP in the myelin fraction from P22 brain homogenates did not significantly differ among the six genotypes, with the exception of a mildly reduced expression in WT mice compared to *GalNAc-T*$^{-/-}$ genotypes (**data not shown**). A significant reduction in MAG protein level was observed in the myelin fraction from *CST*$^{-/-}$ *x GalNAc-T*$^{-/-}$ mice compared to all genotypes, which did not significantly differ from one another (one-way ANOVA $F(5,16) = 7.735$, $p=0.0007$) (**Figure 7A**). Conversely, MAG expression in whole brain homogenates and in optic nerve sections was comparably reduced in all genotypes compared to wild type, suggesting an enhanced loss of appropriate trafficking or site-specific anchoring in [m19]myelin in the *CST*$^{-/-}$*x GalNAc-T*$^{-/-}$ mice (WB: one-way ANOVA $F(5,18) = 13.87$, $p<0.0001$; immunostaining [m20][RM21][m22][RM23]one-way ANOVA $F(5,12) = 13.36$, $p = 0.0001$) (**Figure 7A & B**). This notion is strengthened by the comparable expression of oligodendrocyte transcription factor 2 (Olig2) among genotypes which indicates oligodendrocyte number is normal and oligodendrocytes are not lost due to glycolipid deficiency (one-way ANOVA $F(5,12) = 0.41$, $p = 0.835$)(**Figure 7A**). Myelin NF155 protein levels were significantly reduced to a comparable level in all genotypes deficient in sulfatide, which corresponds with our immunostaining data and previous reports (one-way ANOVA $F(5,18) = 23.41$, $p<0.0001$) (**Figure 7A**). This is replicated in the whole brain extract (**data not shown**).

Discussion (1500 words max)

- The discussion section should be as concise as possible
- brief statement of the principal findings
- discussion of the validity of the observations
- discussion of the findings in light of other published work dealing with the same or closely related subjects
- statement of the possible significance of the work
- Extensive discussion of the literature is discouraged

Glycosphingolipids including sulfatide and complex gangliosides have a significant role in myelinated nerve maintenance, but their distinct or interdependent roles and interactions are unclear. The neurodegenerative consequence of deficiency in either sulfatides or complex ganglioside synthesis through transgenic manipulation indicates a role for these lipids in maintaining myelin and axonal integrity, particularly at the node of Ranvier (Takamiya et al., 1996; Sheikh et al., 1999; Honke et al., 2002; Ishibashi et al., 2002; Marcus et al., 2002; Hoshi et al., 2007; Susuki et al., 2007). It was the aim of this study to investigate their interdependency on interacting membranes in order to add insight to the role each family of lipids plays in myelinated nerve and nodal stability.

We found that interbreeding sulfatide deficient mice with complex ganglioside deficient mice resulted in an exaggerated neurodegenerative phenotype and early death compared to single null mice. Through a combination of ultrastructural, immunohistological, functional, and biochemical studies, we showed that the combined loss of both groups of lipids resulted in a more severe outcome than single lipid deficiency (Takamiya et al., 1996; Honke et al., 2002). Diminishing expression of lipids divided the survival of the seven genotypes produced for this study into three broad groups: Mild (WT and *GalNAc-T*$^{-/-}$); Intermediate (*CST*$^{-/-}$, *CST*$^{-/-}$ *x GalNAc-T*$^{-/-}$*-Tg(neuronal*));

Severe (*CST*$^{-/-}$ *x GD3s*$^{-/-}$, *CST*$^{-/-}$ *x GalNAc-T*$^{-/-}$*-Tg(glial*), *CST*$^{-/-}$ *x GalNAc-T*$^{-/-}$). We reported a more pronounced phenotype in the CNS than the PNS and thereby focused much of our analysis on the CNS. Degenerate axon number increased with diminishing lipid content and conduction became increasingly impaired; MAG expression in the myelin fraction from brain homogenates was significantly lower in the *CST*$^{-/-}$ *x GalNAc-T*$^{-/-}$ genotype compared to all other genotypes; and Nav channel cluster number, Caspr dimer number and Nav channels flanked by NF155 dimers decreased with decreasing lipid expression. Rescuing the neuronal, but not the glial complex ganglioside expression reversed the lethality observed in the double null mice. Examining the relative importance of a- and b-series gangliosides we observed only modest improvement occurred with global a-series ganglioside expression on a sulfatide null background. Collectively, these data indicate the importance of neuronal *b-series* gangliosides (e.g. GD1b, GT1b) in maintaining survival in the co-presence of sulfatide deficiency and indicate interdependency between the functions of these two groups of lipids. We thus propose that sulfatide and b-series ganglioside lipid domains on opposing membranes majorly contribute to a co-ordinated axo-glial adhesion and paranodal organisation, a combined loss of which leads to severe impairment of nerve integrity with a fatal outcome at an early age.

We have previously highlighted the significance of neuronal complex ganglioside expression to nerve integrity in the *GalNAc-T*$^{-/-}$ age-dependent neurodegenerative genotype (Yao et al., 2014). Considering the impact of neuronal ganglioside expression on survival, combined with the reduction of MAG in the myelin fraction in double deficient mice, these findings suggest an underlying mechanism for the lethal phenotype in *CST*$^{-/-}$ *x GalNAc-T*$^{-/-}$ mice. The complex gangliosides GD1a and GT1b are prominently expressed on the axonal membrane and are receptors for MAG (Collins et al., 1997; Vinson et al., 2001). MAG is expressed on the periaxonal membrane of the myelin sheath (Bartsch et al., 1989; Trapp et al., 1989) and is involved in the continuous axo-glial contact and bidirectional signalling along the myelinated nerve, particularly at the paranode. MAG null mice form *cis* bonds in the myelin membrane that are stabilised by *trans* interactions with gangliosides in the

neuronal membrane (Pronker et al., 2016). MAG null mice exhibit delayed maturation of nodes and, similar to *GalNAc-T*$^{-/-}$ mice, modest nervous system abnormalities, suggesting a role in myelinated nerve maintenance rather than development (Montag et al., 1994; Li et al., 1998; Marcus et al., 2002; Pan et al., 2005). Previously it has been shown that MAG levels are reduced in *GalNAc-T*$^{-/-}$ mice (Sheikh et al., 1999; Kawai et al., 2001), and when considered with the comparable phenotype between *GalNAc-T*$^{-/-}$ and *MAG*$^{-/-}$ mice suggests complex gangliosides and MAG cooperatively contribute to the stability of the axo-glial junction[m24][RM25]. Indeed[m26], interbreeding *GalNAc-T*$^{-/-}$ and *MAG*$^{-/-}$ strains did not exacerbate the phenotype of the single null mice, suggesting a complementary and functional interaction between these molecules (Pan et al., 2005). Conversely, in our study, combining *GalNAc-T*$^{-/-}$ and *CST*$^{-/-}$ strains exacerbates the phenotype suggesting two independent roles. Notably, MAG acts as a myelin receptor for axonal gangliosides, and is localised to the myelin membrane by sulfatide rich lipid rafts. Recent analysis of protein extracts from 4-week old sulfatide null mouse brains confirmed a progressive reduction in MAG and a significant reduction in NF155 (25% compared to wild type)(Palavicini et al., 2016). Taken together with extraction studies that identified sulfatide-containing lipid rafts as anchors for MAG and NF155 (Pomicter et al., 2013), it seems that sulfatide acts as a wide-ranging anchor for multiple myelin and glial membrane proteins. With the knowledge that MAG and sulfatide modulate axo-glial stability, Marcus et al. (2002) investigated the significance of both molecules to axo-glial integrity by crossing MAG deficient mice with GalC/sulfatide double deficient mice, which individually have similar phenotypes. Similar to our lethal sulfatide and ganglioside double deficiency phenotype, this genetic combination resulted in a lethal phenotype, with survival up to P22 (Marcus et al., 2002). Again, the NoR appear to develop normally followed by subsequent generalised impairment of the paranodal axo-glial junction. Unlike the minimal effect of combined MAG and complex ganglioside disruption, MAG and ceramide galactosyltransferase (CGT) double deficiency aggravates the phenotype suggesting two non-redundant functions are impaired. This phenotype corresponds to our lethal phenotype, indicating that a loss of interaction between MAG and gangliosides in a membrane environment devoid of GalC

and sulfatide is fatal. It is likely that GalC/sulfatide has a role in promoting localisation/anchoring of MAG and subsequently MAG/ganglioside promote axo-glial integrity. Indeed, we reported a striking deficiency in MAG in the myelin fraction of our double null mice compared to all other genotypes owing to the loss of its localising agent, sulfatide, and binding partner, complex gangliosides.

The severe neurodegenerative phenotype of our double lipid deficient mice reflected that of paranodal protein deficient mice (Tait et al., 2000; Bhat et al., 2001; Boyle et al., 2001; Charles et al., 2002), suggesting an essential role for lipids in paranodal protein maintenance. In the current study we restricted our investigation of nodal disruption to those proteins related to function (Nav channels) or previously identified as lipid raft associated (NF155, Caspr)(Sheikh et al., 1999; Schafer et al., 2004; Susuki et al., 2007; Pomicter et al., 2013) and acknowledge that this was not an exhaustive study. Adhesion molecules freely diffuse in the axon membrane and accumulate at NoR, whereas ion channels and components of the cytoskeleton require transport (Zhang et al., 2012). NF186 is essential for maintenance of the Nav channel clusters at the NoR (Zhang et al., 2012; Desmazieres et al., 2014; Taylor et al., 2017) and appeared unperturbed in our double null mice. This aligns with the fact that NF186 is likely not raft-associated (Schafer et al., 2004; Susuki et al., 2007). ~~Intact~~ The presence of NF186 accounts for the relatively minimal reduction in Na channel clusters and impairment in conduction observed in *CST*$^{-/-}$ *x GalNAc-T*$^{-/-}$ mice. Schafer et al. (2004) proposed an indirect mechanism of axo-glial junction stabilisation at the paranode whereby glycosphingolipid-rich lipid rafts cluster NF155 that then co-cluster with axonal binding partners Caspr and contactin. Indeed, we confirmed by immunostaining and western blot that NF155 was disrupted in all genotypes with sulfatide deficiency. The axonal partner of NF155, Caspr, was also disrupted as had previously been shown in single ganglioside and sulfatide deficiency (Ishibashi et al., 2002; Susuki et al., 2007), but to a greater degree when both sets of lipids were absent. Caspr has been associated with ganglioside-rich lipid rafts on the axonal membrane and in their absence, Caspr is not anchored (Susuki et al., 2007). Our results that the PNS was less perturbed than CNS likely reflects the greater stability of the peripheral node of Ranvier, and greater influence that the paranode has on stability

in the CNS (Rasband and Peles, 2015). However, the combined absence of both NF155 and Caspr through loss of both sulfatide and gangliosides, respectively, likely intensifies the reduction in Nav channel clusters and ultimately leads to enhanced nodal instability compared to single lipid null mice.

Ganglioside, sulfatide and MAG single deficient mice do not exhibit a severe phenotype, strongly suggesting redundant functions: overexpression/loss of other lipids (e.g. simple gangliosides, seminolipid) could, in theory, contribute to the overall phenotype in transgenic mice. Mice that lack the GD3 synthase (GD3s) enzyme that underlies production of all b-series gangliosides (Figure 1A) have grossly normal nodal architecture (Okada et al., 2002), demonstrating that there is compensation in the ganglioside family. It is possible that ganglioside deficient mice have a less severe phenotype than those lacking sulfatide due to compensation by over-expression of simple gangliosides, notably GM3 & GD3 whose levels are markedly elevated in the *GalNAc-T*$^{-/-}$ phenotype (Susuki et al., 2007). The increased severity of double ganglioside null (GM3 only) mice (Kawai et al., 2001; Inoue et al., 2002; Yamashita et al., 2005) lends support for this theory, however, the nodal protein organisation has not been characterised. It was therefore an unexpected finding that the *CST*$^{-/-}$ *x GD3s*$^{-/-}$ strain had such a severe phenotype. This could be thus explained by the lack of the b-series ganglioside GT1b interacting with MAG (Vinson et al., 2001).

It is clear from these results that sulfatide and complex gangliosides have crucial and independent roles in clustering proteins on opposing membranes which is essential to normal axo-glial integrity and nervous system function. Redundant features can compensate for the loss of one family, but their simultaneous absence leads to a catastrophic ~~accumulation of~~ axon degeneration, axo-glial disruption and nodal pathology, culminating in early ~~fatality~~death. (1617 words, 117 over)

Figure legends

Figure 1. Generation of lipid deficient transgenic mouse lines and confirmation by PCR and immunostaining. Six mouse lines were used and generated: Wild type; *GalNAc-T$^{-/-}$; CST$^{-/-}$, CST$^{-/-}$ x GalNAc-T$^{-/-}$-Tg(neuronal); CST$^{-/-}$ x GD3s$^{-/-}$; CST$^{-/-}$ x GalNAc-T$^{-/-}$.* A) Sulfatide and ganglioside biosynthesis pathways (associated gene knock outs are indicated in boxes). Ceramide is the precursor to sulfatide and gangliosides. The cerebroside sulfotransferase (CST) enzyme is necessary for the synthesis of sulfatide from galactocerebroside (GalC). The GalNAc-transferase (GalNAc-T) enzyme is necessary for generation of complex gangliosides and the GD3 synthase (GD3s) enzyme for specific production of a-series complex ganglioside. Constructs were generated to drive GalNAc-T expression in neurons of *GalNAc-T$^{-/-}$ x CST$^{-/-}$* mice to produce the *GalNAc-T$^{-/-}$-Tg(neuronal)* mouse line. Location of MAG binding site to terminal 2,3 sialic acid is indicated by a red circle. B) PCR results confirm presence or absence of GalNAc-T, GD3s and CST expression in mouse lines. Large bands represent the disrupted GalNAc-T and CST gene with insert, while the smaller band represents the disruption of the GD3s gene. The flag identifies the re-introduction of the GalNAc-T gene into the neurons. C) Expression of a- and b- series gangliosides and sulfatide was confirmed by staining peripheral nerves with anti-GM1, anti-GD1b and anti-sulfatide monoclonal antibodies (green), respectively. Axons and myelin were identified with neurofilament or MBP (red), respectively. Scale bar = 10 μm.

Figure 2. Altering the expression of gangliosides and sulfatide in novel transgenic mouse lines effects survival and phenotype. A) The weight of double null (n=10) and *CST$^{-/-}$ x GD3s$^{-/-}$* (n=6) mice is normal during development, but declines from P15-25 and is significantly reduced compared to other genotypes at P22. Statistical differences among genotypes were determined by one-way ANOVA followed by Tukey's *post-hoc* tests to compare multiple comparisons, indicated on the graphs as

follows: *p<0.05; **p<0.01; ***p<0.001. B) *CST$^{-/-}$ x GalNAc-T$^{-/-}$* and *CST$^{-/-}$ x GD3s$^{-/-}$* mice display a reduction in stature, hindlimb leg splaying, a hunched appearance and tremor at P22. Gross brain anatomy does not differ between genotypes. C) Survival plots demonstrate that incrementally diminishing ganglioside and sulfatide expression corresponds with a reduction in life expectancy up to 25 weeks. Wild type (n=7) and GalNAc-T$^{-/-}$ (n=10) mice have a normal life expectancy. In the absence of sulfatide with normal ganglioside expression life expectancy to 25 weeks is more than halved in *CST$^{-/-}$* mice (n=18). Interestingly, in the absence of sulfatide and complex gangliosides with the reintroduction of complex gangliosides into neurons alone (n=6), life expectancy is improved with 60% of mice surviving to 25 weeks and beyond. Mice with no sulfatide and a-series gangliosides expressed globally (n=38) can survive up to 20 weeks. Double ganglioside and sulfatide knock out mice (n=29) have the worst phenotype, never surviving past 4 weeks and with death occurring at P21-25. Reintroduction of gangliosides into glial (n=12) does not improve survival.

Figure 3. The additional loss of complex gangliosides on a sulfatide null background does not augment disorganisation at the node of Ranvier or electrophysiological function in the peripheral nervous system. A) There is modest Nav1.6 channel cluster lengthening in both *CST$^{-/-}$* and *CST$^{-/-}$ x GalNAc-T$^{-/-}$* teased sciatic nerve that does not reach significance. Invasion of the sciatic nerve paranode by Kv1.1 channels, shown by a decrease in the gap between positive domains, is significantly and comparably enhanced in both *CST$^{-/-}$* and *CST$^{-/-}$ x GalNAc-T$^{-/-}$* mice compared to WT and GalNAc-T$^{-/-}$ nodes of Ranvier. The length of pan-neurofascin immunostained domains does not significantly differ among genotypes. Representative images are shown of sciatic nerve sections from each genotype immunostained for Nav1.6 or anti-Kv1.1 antibody. Nav channel clusters were observed and appeared similar in every genotype. Kv1.1 formed two distinct domains of immunostaining at the juxtaparanodes in WT and *GalNAcT$^{-/-}$* mice. Conversely, mice lacking sulfatide expression had Kv1.1 staining at the paranodes, suggesting disruption to the axo-glial junction. (WT

n=3, *GalNAc-T*$^{-/-}$ n=3, *CST*$^{-/-}$ n=3, *CST*$^{-/-}$ *x GalNAc-T*$^{-/-}$ n=4 Scale bar = 5 µm. B) Perineural recordings of Nav and Kv channel currents from intercostal nerves showed an increase in recovery time for both peaks following paired pulse stimulation in both *CST*$^{-/-}$ and *CST*$^{-/-}$ *x GalNAc-T*$^{-/-}$ mice compared to WT and *GalNAc-T*$^{-/-}$ mice. The *CST*$^{-/-}$ and *CST*$^{-/-}$ *x GalNAc-T*$^{-/-}$ mice were not significantly different from each other at any interstimulus interval. Graphs display the means and ±SEM for each genotype (WT n=5, *GalNAc-T*$^{-/-}$ n=2, *CST*$^{-/-}$ n=3, *CST*$^{-/-}$ *x GalNAc-T*$^{-/-}$ n=2), and statistical analysis performed (two-way ANOVA; # signifies WT vs. *CST*$^{-/-}$ *x GalNAc-T*$^{-/-}$ mice; * signifies WT vs *CST*$^{-/-}$; + signifies *GalNAc-T*$^{-/-}$ vs *CST*$^{-/-}$ *x GalNAc-T*$^{-/-}$; ^ signifies *GalNAc-T*$^{-/-}$ vs *CST*$^{-/-}$ *x GalNAc-T*$^{-/-}$). Sciatic nerve conduction velocity decreased in *CST*$^{-/-}$(n=4), *GalNAc-T*$^{-/-}$ (n=4) and *CST*$^{-/-}$ *x GalNAc-T*$^{-/-}$ (n=5) mice compared to wild type (n=3), but only reached significance in *CST*$^{-/-}$ nerve. C) Peripheral nerve MAG immunostaining was comparable among genotypes. Scale bar = 20 µm. Graphs display the means and ±SEM for each genotype,), and statistical analysis performed (one-way ANOVA followed by Tukey's *post-hoc* tests to compare multiple comparisons, indicated on the graphs as follows: *p<0.05; **p<0.01; ***p<0.001).

Figure 4. Loss of both sulfatide and complex gangliosides results in a modest reduction in CNS Nav channel cluster number and sulfatide deficiency reduces NF155 presence at parnodal loops. A) The number of Nav channel clusters significantly decreases in glycolipid deficient mouse optic nerves (n=3-4/genotype). Reintroducing a- and b-series gangliosides into neurons rescues this feature. B) Nav channel clusters flanked by normal paranodal neurofascin are significantly reduced in number when sulfatide is not expressed (n=2-3/genotype). Box-and whisker plots are used to display the spread of all data points collected from each animal then means were calculated per genotype for statistical analysis (one-way ANOVA followed by Tukey's *post-hoc* tests to compare multiple comparisons, indicated on the graphs as follows: *p<0.05; **p<0.01; ***p<0.001). C) Representative images of optic nerve sections from each genotype double-immunostained for pan-voltage gated

688 sodium channel (pNav) antibody (green) and pan-neurofascin (pNFasc) antibody (red). Na channel
689 clusters were observed in every genotype. pNFasc immunostaining formed a long band crossing the
690 node and paranodes in WT and *GalNAc-T*$^{-/-}$ mice suggesting labelling of the NF186 and NF155
691 isoforms, respectively. All of the genotypes lacking sulfatide expression had pNFasc staining
692 restricted to the node of Ranvier and co-localising only with pNav staining, suggesting presence of
693 only the NF186 isoform of neurofascin. Scale bar = 5 μm.

694

695 **Figure 5**. Paranodal Caspr dimer immunostaining in CNS tissue is progressively reduced with
696 increasing glycolipid deficiency. A) *CST*$^{-/-}$ *x GalNAc-T*$^{-/-}$ and *CST*$^{-/-}$ *x GD3s*$^{-/-}$ mice have significantly
697 fewer Caspr dimers per field of view (FOV) compared to WT and *GalNAc-T*$^{-/-}$ mice, and are not
698 significantly different to each other (n=2-5/genotype). Caspr dimer number is improved to levels
699 within *GalNAc-T*$^{-/-}$ mice range, but not WT, in *CST*$^{-/-}$ and *CST*$^{-/-}$ x *GalNAc-T*$^{-/-}$*-Tg(neuronal)* mice, which
700 both display significantly more Caspr dimers than *CST*$^{-/-}$ *x GalNAc-T*$^{-/-}$ mice. Box-and whisker plots
701 are used to display the spread of all data points collected from each animal then means were
702 calculated per genotype for statistical analysis (one-way ANOVA followed by Tukey's *post-hoc* tests
703 to compare multiple comparisons, indicated on the graphs as follows: *p<0.05; **p<0.01;
704 ***p<0.001). B) Representative images of optic nerve sections from each genotype double-
705 immunostained for Caspr (red) and nodal marker AnkyrinG (green) show the reduction in Caspr
706 dimer number with diminishing glycolipid expression. Scale bar = 10 μm.

707

708 **Figure 6**. Glycolipid deficiency reduces CNS axon survival and function. A) Degenerate axon number
709 increases to a significant level compared to wild type in optic nerves from *CST*$^{-/-}$, *CST*$^{-/-}$ *x GD3s*$^{-/-}$ and
710 *CST*$^{-/-}$ *x GalNAc-T*$^{-/-}$ mice. Reintroducing a- and b-series gangliosides into neurons rescues this
711 pathology. B) Electron micrographs depict the differences among the genotypes: white arrowheads
712 indicate degenerate axons. Myelin is similar among mouse lines. One-way ANOVA followed by

Tukey's post-hoc tests to compare multiple comparisons, indicated on the graphs as follows: *p<0.05; **p<0.01; ***p<0.001. Scale bar = 2 µm C) A reduction in conduction velocity was observed in optic nerves with diminishing glycolipid content. Representative CAP traces from each genotype show the normal waveform in *WT*, *GalNAc-T$^{-/-}$* and *CST$^{-/-}$ x GalNAc-T$^{-/-}$-Tg(neuronal)* optic nerves, however the waveform becomes abnormal in the *CST$^{-/-}$, CST$^{-/-}$ x GD3s$^{-/-}$* and *CST$^{-/-}$ x GalNAc-T$^{-/-}$* mice. Horizontal scale bar = 2 ms, vertical scale bar = 1 mV.

Figure 7. *N.B. New order of genotypes*. MAG and NF155 expression in the myelin fraction is altered by glycolipid deficiency. A) In the myelin fraction from P22 brain homogenates, MAG is significantly reduced in *CST$^{-/-}$ x GalNAc-T$^{-/-}$* mice compared to all genotypes, which do not significantly differ from one another (upper graph). All genotypes have a significant reduction in MAG expression in whole brain homogenate compared to WT (middle graph). Myelin NF155 was significantly reduced in all genotypes compared to WT (indicated by *) and *GalNAc-T$^{-/-}$* (indicated by #), which had similar levels (lower graph). ^indicates significant difference between *CST$^{-/-}$ x GalNAc-T$^{-/-}$* and *CST$^{-/-}$ x GalNAc-T$^{-/-}$-Tg(neuronal)* mice. Olig2 is unchanged by altered glycolipid expression. Representative blots show protein intensity per genotype, indicated by the corresponding number indicated in the key. B) P22 optic nerve MAG immunostaining is significantly reduced in all genotypes compared to *wild type* nerve, which do not significantly differ from one another. Representative images show MAG immunostaining per genotype. Means were calculated per genotype for statistical analysis (one-way ANOVA followed by Tukey's *post-hoc* tests to compare multiple comparisons, indicated on the graphs as follows: *p<0.05; **p<0.01; ***p<0.001). Scale bar = 50 µm.

Figure 8. Schematic depicting the glycolipid rafts and their associated paranodal proteins Caspr, NF155 and MAG under wild type conditions and in our transgenic mouse lines. GD1a and GT1b are represented in the ganglioside rafts as they are the major ligands of MAG, however, in reality the

rafts would contain all complex gangliosides. Normally GD1a and GT1b in rafts will tether MAG but in their absence MAG does not make the axo-glial connection. If NF155 is present, this protein can partner with Caspr/Contactin to make an axo-glial junction. However, when sulfatide is absent, NF155 is also lost from the paranode. In the absence of NF155, Caspr presence is also diminished, especially with loss of complex ganglioside rafts. Under conditions of both ganglioside and sulfatide raft deficiency, we propose an absence of the structurally supporting proteins MAG and NF155 that results in the loss of a functionally competent axo-glial junction.

Acknowledgements

Include funding sources, John Dempster

References

Barrie JA, Montague P, Karim S, Kirkham D, Nave KA, Anderson TJ, Griffiths IR, McLaughlin M (2010) Modulation of rumpshaker phenotype with wild-type PLP/DM20 suggests several pathogenic mechanisms. Journal of neuroscience research 88:2135-2145.

Bartsch U, Kirchhoff F, Schachner M (1989) Immunohistological localization of the adhesion molecules L1, N-CAM, and MAG in the developing and adult optic nerve of mice. The Journal of comparative neurology 284:451-462.

Bhat MA, Rios JC, Lu Y, Garcia-Fresco GP, Ching W, St Martin M, Li J, Einheber S, Chesler M, Rosenbluth J, Salzer JL, Bellen HJ (2001) Axon-glia interactions and the domain organization of myelinated axons requires neurexin IV/Caspr/Paranodin. Neuron 30:369-383.

Boffey J, Odaka M, Nicoll D, Wagner ER, Townson K, Bowes T, Conner J, Furukawa K, Willison HJ (2005) Characterisation of the immunoglobulin variable region gene usage encoding the murine anti-ganglioside antibody repertoire. Journal of neuroimmunology 165:92-103.

Bowes T, Wagner ER, Boffey J, Nicholl D, Cochrane L, Benboubetra M, Conner J, Furukawa K, Furukawa K, Willison HJ (2002) Tolerance to self gangliosides is the major factor restricting the antibody response to lipopolysaccharide core oligosaccharides in Campylobacter jejuni strains associated with Guillain-Barre syndrome. Infection and immunity 70:5008-5018.

Boyle ME, Berglund EO, Murai KK, Weber L, Peles E, Ranscht B (2001) Contactin orchestrates assembly of the septate-like junctions at the paranode in myelinated peripheral nerve. Neuron 30:385-397.

Braga MF, Harvey AL, Rowan EG (1991) Effects of tacrine, velnacrine (HP029), suronacrine (HP128), and 3,4-diaminopyridine on skeletal neuromuscular transmission in vitro. British journal of pharmacology 102:909-915.

Charles P, Tait S, Faivre-Sarrailh C, Barbin G, Gunn-Moore F, Denisenko-Nehrbass N, Guennoc AM, Girault JA, Brophy PJ, Lubetzki C (2002) Neurofascin is a glial receptor for the paranodin/Caspr-contactin axonal complex at the axoglial junction. Current biology : CB 12:217-220.

Collins BE, Yang LJ, Mukhopadhyay G, Filbin MT, Kiso M, Hasegawa A, Schnaar RL (1997) Sialic acid specificity of myelin-associated glycoprotein binding. The Journal of biological chemistry 272:1248-1255.

Desmazieres A, Zonta B, Zhang A, Wu LM, Sherman DL, Brophy PJ (2014) Differential stability of PNS and CNS nodal complexes when neuronal neurofascin is lost. The Journal of neuroscience : the official journal of the Society for Neuroscience 34:5083-5088.

Dupree JL, Girault JA, Popko B (1999) Axo-glial interactions regulate the localization of axonal paranodal proteins. The Journal of cell biology 147:1145-1152.

Garcia-Fresco GP, Sousa AD, Pillai AM, Moy SS, Crawley JN, Tessarollo L, Dupree JL, Bhat MA (2006) Disruption of axo-glial junctions causes cytoskeletal disorganization and degeneration of Purkinje neuron axons. Proceedings of the National Academy of Sciences of the United States of America 103:5137-5142.

Griffiths IR, Duncan ID, McCulloch M (1981) Shaking pups: a disorder of central myelination in the spaniel dog. II. Ultrastructural observations on the white matter of the cervical spinal cord. Journal of neurocytology 10:847-858.

Honke K, Hirahara Y, Dupree J, Suzuki K, Popko B, Fukushima K, Fukushima J, Nagasawa T, Yoshida N, Wada Y, Taniguchi N (2002) Paranodal junction formation and spermatogenesis require sulfoglycolipids. Proceedings of the National Academy of Sciences of the United States of America 99:4227-4232.

Hoshi T, Suzuki A, Hayashi S, Tohyama K, Hayashi A, Yamaguchi Y, Takeuchi K, Baba H (2007) Nodal protrusions, increased Schmidt-Lanterman incisures, and paranodal disorganization are characteristic features of sulfatide-deficient peripheral nerves. Glia 55:584-594.

Inoue M, Fujii Y, Furukawa K, Okada M, Okumura K, Hayakawa T, Furukawa K, Sugiura Y (2002) Refractory skin injury in complex knock-out mice expressing only the GM3 ganglioside. The Journal of biological chemistry 277:29881-29888.

Ishibashi T, Dupree JL, Ikenaka K, Hirahara Y, Honke K, Peles E, Popko B, Suzuki K, Nishino H, Baba H (2002) A myelin galactolipid, sulfatide, is essential for maintenance of ion channels on myelinated axon but not essential for initial cluster formation. The Journal of neuroscience : the official journal of the Society for Neuroscience 22:6507-6514.

Ishizuka I (1997) Chemistry and functional distribution of sulfoglycolipids. Progress in lipid research 36:245-319.

Jackman N, Ishii A, Bansal R (2009) Oligodendrocyte development and myelin biogenesis: parsing out the roles of glycosphingolipids. Physiology (Bethesda, Md) 24:290-297.

Kawai H, Allende ML, Wada R, Kono M, Sango K, Deng C, Miyakawa T, Crawley JN, Werth N, Bierfreund U, Sandhoff K, Proia RL (2001) Mice expressing only monosialoganglioside GM3 exhibit lethal audiogenic seizures. The Journal of biological chemistry 276:6885-6888.

Li C, Trapp B, Ludwin S, Peterson A, Roder J (1998) Myelin associated glycoprotein modulates glia-axon contact in vivo. Journal of neuroscience research 51:210-217.

Marcus J, Dupree JL, Popko B (2002) Myelin-associated glycoprotein and myelin galactolipids stabilize developing axo-glial interactions. The Journal of cell biology 156:567-577.

Marcus J, Honigbaum S, Shroff S, Honke K, Rosenbluth J, Dupree JL (2006) Sulfatide is essential for the maintenance of CNS myelin and axon structure. Glia 53:372-381.

McGonigal R, Rowan EG, Greenshields KN, Halstead SK, Humphreys PD, Rother RP, Furukawa K, Willison HJ (2010) Anti-GD1a antibodies activate complement and calpain to injure distal motor nodes of Ranvier in mice. Brain 133:1944-1960.

Montag D, Giese KP, Bartsch U, Martini R, Lang Y, Bluthmann H, Karthigasan J, Kirschner DA, Wintergerst ES, Nave KA, et al. (1994) Mice deficient for the myelin-associated glycoprotein show subtle abnormalities in myelin. Neuron 13:229-246.

Norton WT, Poduslo SE (1973) Myelination in rat brain: changes in myelin composition during brain maturation. Journal of neurochemistry 21:759-773.

Okada M, Itoh Mi M, Haraguchi M, Okajima T, Inoue M, Oishi H, Matsuda Y, Iwamoto T, Kawano T, Fukumoto S, Miyazaki H, Furukawa K, Aizawa S, Furukawa K (2002) b-series Ganglioside deficiency exhibits no definite changes in the neurogenesis and the sensitivity to Fas-mediated apoptosis but impairs regeneration of the lesioned hypoglossal nerve. The Journal of biological chemistry 277:1633-1636.

Palavicini JP, Wang C, Chen L, Ahmar S, Higuera JD, Dupree JL, Han X (2016) Novel molecular insights into the critical role of sulfatide in myelin maintenance/function. Journal of neurochemistry 139:40-54.

Pan B, Fromholt SE, Hess EJ, Crawford TO, Griffin JW, Sheikh KA, Schnaar RL (2005) Myelin-associated glycoprotein and complementary axonal ligands, gangliosides, mediate axon stability in the CNS and PNS: neuropathology and behavioral deficits in single- and double-null mice. Experimental neurology 195:208-217.

Pillai AM, Thaxton C, Pribisko AL, Cheng JG, Dupree JL, Bhat MA (2009) Spatiotemporal ablation of myelinating glia-specific neurofascin (Nfasc NF155) in mice reveals gradual loss of paranodal axoglial junctions and concomitant disorganization of axonal domains. Journal of neuroscience research 87:1773-1793.

Poliak S, Peles E (2003) The local differentiation of myelinated axons at nodes of Ranvier. Nature reviews Neuroscience 4:968-980.

Pomicter AD, Deloyht JM, Hackett AR, Purdie N, Sato-Bigbee C, Henderson SC, Dupree JL (2013) Nfasc155H and MAG are specifically susceptible to detergent extraction in the absence of the myelin sphingolipid sulfatide. Neurochemical research 38:2490-2502.

Pronker MF, Lemstra S, Snijder J, Heck AJ, Thies-Weesie DM, Pasterkamp RJ, Janssen BJ (2016) Structural basis of myelin-associated glycoprotein adhesion and signalling. Nature communications 7:13584.
Rasband MN, Peles E (2015) The Nodes of Ranvier: Molecular Assembly and Maintenance. Cold Spring Harbor perspectives in biology 8:a020495.
Salzer JL (1997) Clustering sodium channels at the node of Ranvier: close encounters of the axon-glia kind. Neuron 18:843-846.
Schafer DP, Bansal R, Hedstrom KL, Pfeiffer SE, Rasband MN (2004) Does paranode formation and maintenance require partitioning of neurofascin 155 into lipid rafts? The Journal of neuroscience : the official journal of the Society for Neuroscience 24:3176-3185.
Sheikh KA, Sun J, Liu Y, Kawai H, Crawford TO, Proia RL, Griffin JW, Schnaar RL (1999) Mice lacking complex gangliosides develop Wallerian degeneration and myelination defects. Proceedings of the National Academy of Sciences of the United States of America 96:7532-7537.
Simons K, Toomre D (2000) Lipid rafts and signal transduction. Nature reviews Molecular cell biology 1:31-39.
Sonnino S, Aureli M, Mauri L, Ciampa MG, Prinetti A (2015) Membrane lipid domains in the nervous system. Frontiers in bioscience (Landmark edition) 20:280-302.
Sonnino S, Aureli M, Grassi S, Mauri L, Prioni S, Prinetti A (2014) Lipid rafts in neurodegeneration and neuroprotection. Molecular neurobiology 50:130-148.
Susuki K, Baba H, Tohyama K, Kanai K, Kuwabara S, Hirata K, Furukawa K, Furukawa K, Rasband MN, Yuki N (2007) Gangliosides contribute to stability of paranodal junctions and ion channel clusters in myelinated nerve fibers. Glia 55:746-757.
Susuki K, Chang KJ, Zollinger DR, Liu Y, Ogawa Y, Eshed-Eisenbach Y, Dours-Zimmermann MT, Oses-Prieto JA, Burlingame AL, Seidenbecher CI, Zimmermann DR, Oohashi T, Peles E, Rasband MN (2013) Three mechanisms assemble central nervous system nodes of Ranvier. Neuron 78:469-482.
Tait S, Gunn-Moore F, Collinson JM, Huang J, Lubetzki C, Pedraza L, Sherman DL, Colman DR, Brophy PJ (2000) An oligodendrocyte cell adhesion molecule at the site of assembly of the paranodal axo-glial junction. The Journal of cell biology 150:657-666.
Takamiya K, Yamamoto A, Furukawa K, Yamashiro S, Shin M, Okada M, Fukumoto S, Haraguchi M, Takeda N, Fujimura K, Sakae M, Kishikawa M, Shiku H, Furukawa K, Aizawa S (1996) Mice with disrupted GM2/GD2 synthase gene lack complex gangliosides but exhibit only subtle defects in their nervous system. Proceedings of the National Academy of Sciences of the United States of America 93:10662-10667.
Taylor AM, Saifetiarova J, Bhat MA (2017) Postnatal Loss of Neuronal and Glial Neurofascins Differentially Affects Node of Ranvier Maintenance and Myelinated Axon Function. Frontiers in cellular neuroscience 11:11.
Trapp BD, Andrews SB, Wong A, O'Connell M, Griffin JW (1989) Co-localization of the myelin-associated glycoprotein and the microfilament components, F-actin and spectrin, in Schwann cells of myelinated nerve fibres. Journal of neurocytology 18:47-60.
Vinson M, Strijbos PJ, Rowles A, Facci L, Moore SE, Simmons DL, Walsh FS (2001) Myelin-associated glycoprotein interacts with ganglioside GT1b. A mechanism for neurite outgrowth inhibition. The Journal of biological chemistry 276:20280-20285.
Yamashita T, Wu YP, Sandhoff R, Werth N, Mizukami H, Ellis JM, Dupree JL, Geyer R, Sandhoff K, Proia RL (2005) Interruption of ganglioside synthesis produces central nervous system degeneration and altered axon-glial interactions. Proceedings of the National Academy of Sciences of the United States of America 102:2725-2730.
Yao D, McGonigal R, Barrie JA, Cappell J, Cunningham ME, Meehan GR, Fewou SN, Edgar JM, Rowan E, Ohmi Y, Furukawa K, Furukawa K, Brophy PJ, Willison HJ (2014) Neuronal expression of GalNAc transferase is sufficient to prevent the age-related neurodegenerative phenotype of

complex ganglioside-deficient mice. The Journal of neuroscience : the official journal of the Society for Neuroscience 34:880-891.

Yool DA, Klugmann M, McLaughlin M, Vouyiouklis DA, Dimou L, Barrie JA, McCulloch MC, Nave KA, Griffiths IR (2001) Myelin proteolipid proteins promote the interaction of oligodendrocytes and axons. Journal of neuroscience research 63:151-164.

Zhang Y, Bekku Y, Dzhashiashvili Y, Armenti S, Meng X, Sasaki Y, Milbrandt J, Salzer JL (2012) Assembly and maintenance of nodes of ranvier rely on distinct sources of proteins and targeting mechanisms. Neuron 73:92-107.

Life expectancy

	GalNAcT enzyme expressed globally	CST enzyme expressed globally	Axonal complex ganglioside expression		Global a-series over expression	Non-neuronal GM3 over-expression	Non-neuronal GD3 over-expression
			a -series	b - series			
Wild type	✓	✓	✓	✓	×	×	×
GalNAcT$^{-/-}$	×	✓	×	×	×	✓	✓
CST$^{-/-}$	✓	×	✓	✓	×	×	×
CST$^{-/-}$ x GalNAcT$^{-/-}$ Tg (neuronal)	×	×	✓	✓	×	✓	✓
CST$^{-/-}$ x GD3s$^{-/-}$	✓	×	✓	×	✓	×	×
CST$^{-/-}$ x GalNAcT$^{-/-}$ Tg(glial)	×	×	×	×	×	✓	✓
CST$^{-/-}$ x GalNAcT$^{-/-}$	×	×	×	×	×	✓	✓

Table 1. Lipid expression profiles of genotypes in this study.

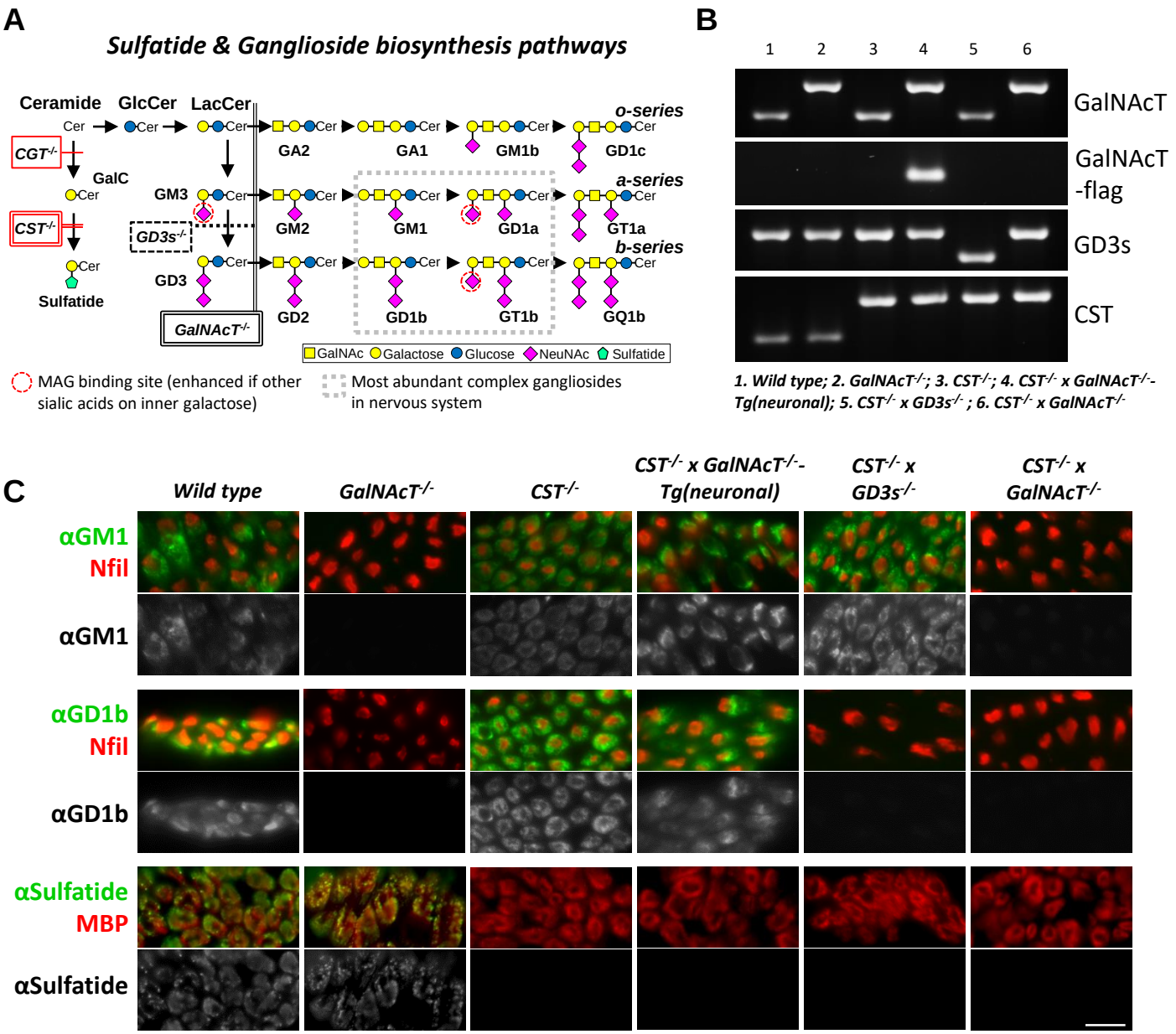

Figure 1. Generation of lipid deficient transgenic mouse lines and confirmation by PCR and immunostaining. Six mouse lines were used and generated: Wild type; *GalNAc-T$^{-/-}$; CST$^{-/-}$, CST$^{-/-}$ x GalNAc-T$^{-/-}$-Tg(neuronal); CST$^{-/-}$ x GD3s$^{-/-}$; CST$^{-/-}$ x GalNAc-T$^{-/-}$.* A) Sulfatide and ganglioside biosynthesis pathways (associated gene knock outs are indicated in boxes). Ceramide is the precursor to sulfatide and gangliosides. The cerebroside sulfotransferase (CST) enzyme is necessary for the synthesis of sulfatide from galactocerebroside (GalC). The GalNAc-transferase (GalNAc-T) enzyme is necessary for generation of complex gangliosides and the GD3 synthase (GD3s) enzyme for specific production of a-series complex ganglioside. Constructs were generated to drive GalNAc-T expression in neurons of *GalNAc-T$^{-/-}$ x CST$^{-/-}$* mice to produce the *GalNAc-T$^{-/-}$-Tg(neuronal)* mouse line. B) PCR results confirm presence or absence of GalNAc-T, GD3s and CST expression in mouse lines. Large bands represent the disrupted GalNAc-T and CST gene with insert, while the smaller band represents the disruption of the GD3s gene. The flag identifies the re-introduction of the GalNAc-T gene into the neurons. C) Expression of a- and b- series gangliosides and sulfatide was confirmed by staining peripheral nerves with anti-GM1, anti-GD1b and anti-sulfatide monoclonal antibodies (green), respectively. Axons and myelin were identified with neurofilament or MBP (red), respectively. Scale bar = 10 µm.

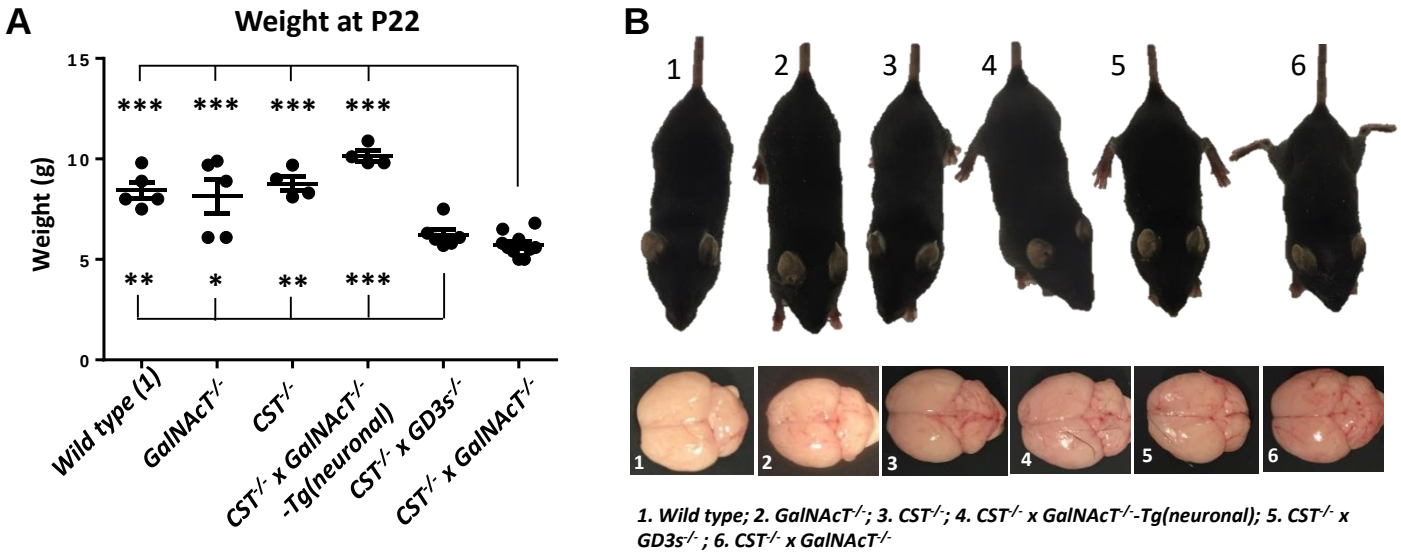

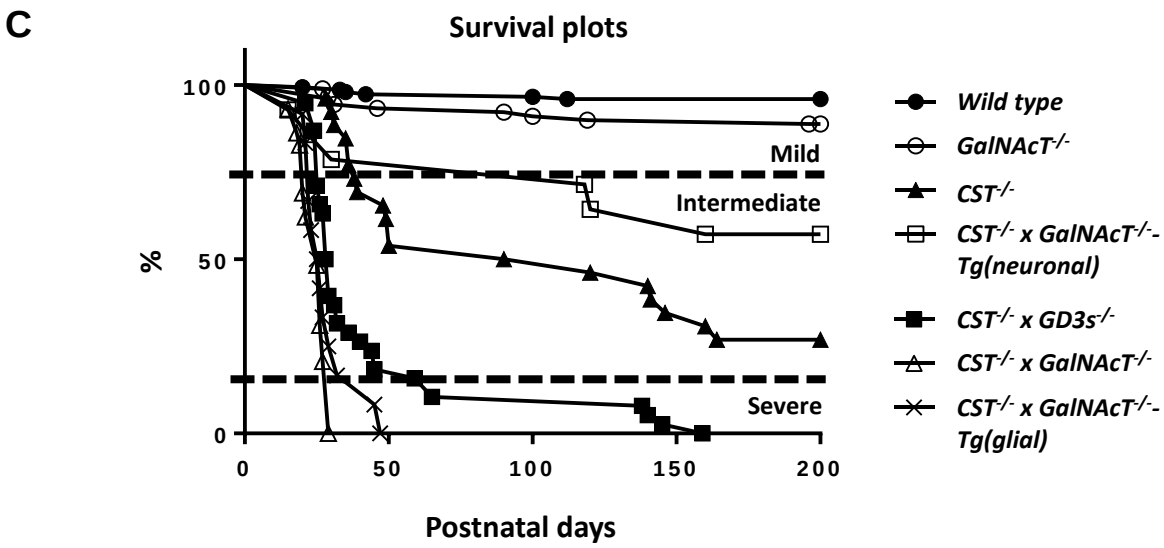

Figure 2. Altering the expression of gangliosides and sulfatide in novel transgenic mouse lines effects survival and phenotype. A) The weight of double null (n=10) and *CST$^{-/-}$ x GD3s$^{-/-}$* (n=6) mice is normal during development, but declines from P15-25 and is significantly reduced compared to other genotypes at P22. Statistical differences among genotypes were determined by one-way ANOVA followed by Tukey's *post-hoc* tests to compare multiple comparisons, indicated on the graphs as follows: *p<0.05; **p<0.01; ***p<0.001. B) *CST$^{-/-}$ x GalNAc-T$^{-/-}$* and *CST$^{-/-}$ x GD3s$^{-/-}$* mice display a reduction in stature, hindlimb leg splaying, a hunched appearance and tremor at P22. Gross brain anatomy does not differ between genotypes. C) Survival plots demonstrate that incrementally diminishing ganglioside and sulfatide expression corresponds with a reduction in life expectancy up to 25 weeks. Wild type (n=7) and GalNAc-T$^{-/-}$ (n=10) mice have a normal life expectancy. In the absence of sulfatide with normal ganglioside expression life expectancy to 25 weeks is more than halved in *CST$^{-/-}$* mice (n=18). Interestingly, in the absence of sulfatide and complex gangliosides with the reintroduction of complex gangliosides into neurons alone (n=6), life expectancy is improved with 60% of mice surviving to 25 weeks and beyond. Mice with no sulfatide and a-series gangliosides expressed globally (n=38) can survive up to 20 weeks. Double ganglioside and sulfatide knock out mice (n=29) have the worst phenotype, never surviving past 4 weeks and with death occurring at P21-25. Reintroduction of gangliosides into glial (n=12) does not improve survival.

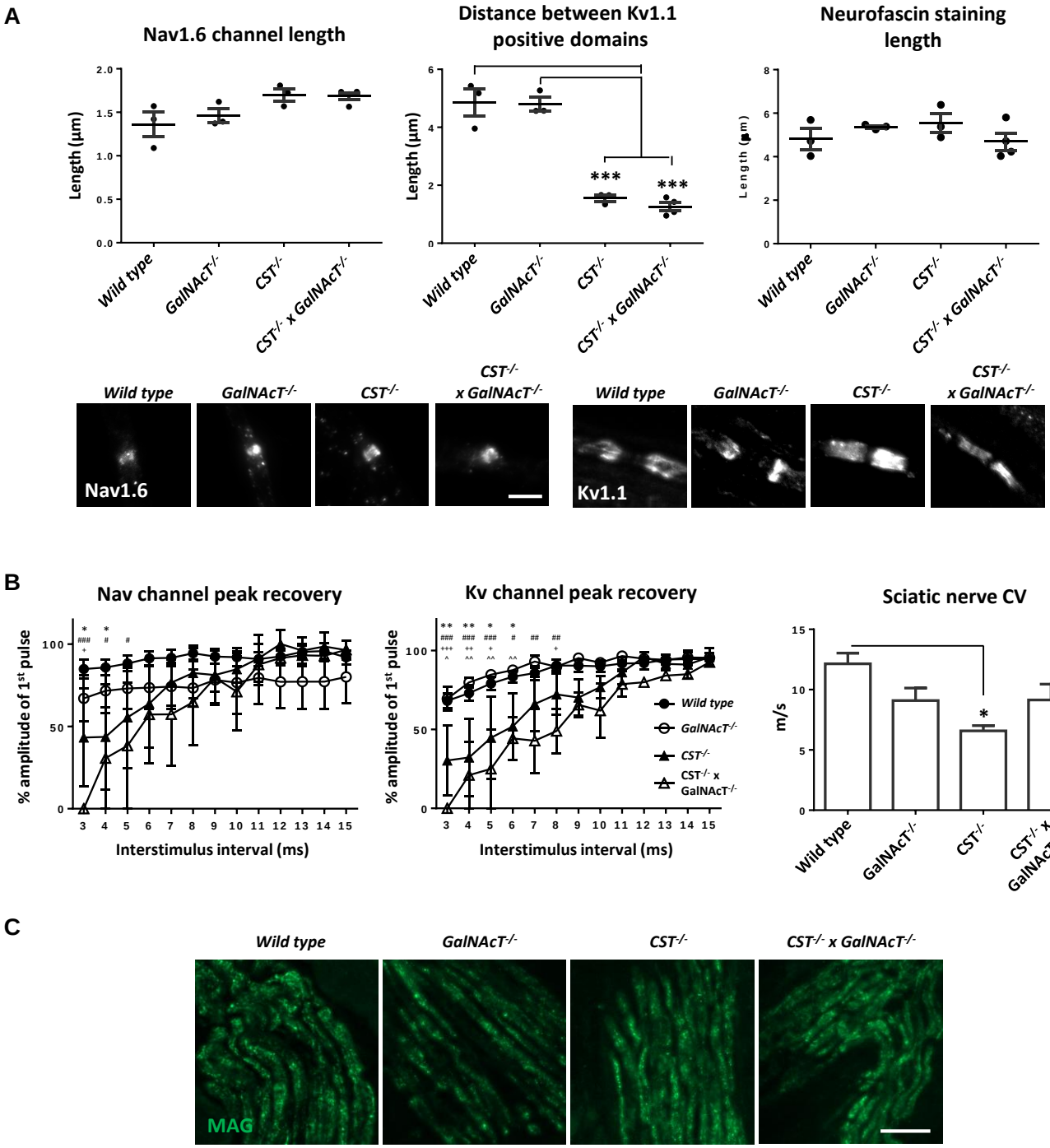

Figure 3. The additional loss of complex gangliosides on a sulfatide null background does not augment disorganisation at the node of Ranvier or electrophysiological function in the peripheral nervous system. A) There is modest Nav1.6 channel cluster lengthening in both *CST$^{-/-}$* and *CST$^{-/-}$ x GalNAc-T$^{-/-}$* teased sciatic nerve that does not reach significance. Invasion of the sciatic nerve paranode by Kv1.1 channels, shown by a decrease in the gap between positive domains, is significantly and comparably enhanced in both *CST$^{-/-}$* and *CST$^{-/-}$ x GalNAc-T$^{-/-}$* mice compared to WT and GalNAc-T$^{-/-}$ nodes of Ranvier. The length of pan-neurofascin immunostained domains does not significantly differ among genotypes. Representative images are shown of sciatic nerve sections from each genotype immunostained for Nav1.6 or anti-Kv1.1 antibody. Nav channel clusters were observed and appeared similar in every genotype. Kv1.1 formed two distinct domains of immunostaining at the juxtaparanodes in WT and *GalNAcT$^{-/-}$* mice. Conversely, mice lacking sulfatide expression had Kv1.1 staining at the paranodes, suggesting disruption to the axo-glial junction. (WT n=3, *GalNAc-T$^{-/-}$* n=3, *CST$^{-/-}$* n=3, *CST$^{-/-}$ x GalNAc-T$^{-/-}$* n=4 Scale bar = 5 µm. B) Perineural recordings of Nav and Kv channel currents from intercostal nerves showed an increase in recovery time for both peaks following paired pulse stimulation in both *CST$^{-/-}$* and *CST$^{-/-}$ x GalNAc-T$^{-/-}$* mice compared to WT and *GalNAc-T$^{-/-}$* mice. The *CST$^{-/-}$* and *CST$^{-/-}$ x GalNAc-T$^{-/-}$* mice were not significantly different from each other at any interstimulus interval. Graphs display the means and ±SEM for each genotype (WT n=5, *GalNAc-T$^{-/-}$* n=2, *CST$^{-/-}$* n=3, *CST$^{-/-}$ x GalNAc-T$^{-/-}$* n=2), and statistical analysis performed (two-way ANOVA; # signifies WT vs. *CST$^{-/-}$ x GalNAc-T$^{-/-}$* mice; * signifies WT vs *CST$^{-/-}$*; + signifies *GalNAc-T$^{-/-}$* vs *CST$^{-/-}$ x GalNAc-T$^{-/-}$*; ^ signifies *GalNAc-T$^{-/-}$* vs *CST$^{-/-}$ x GalNAc-T$^{-/-}$*). Sciatic nerve conduction velocity decreased in *CST$^{-/-}$*(n=4), *GalNAc-T$^{-/-}$* (n=4) and *CST$^{-/-}$ x GalNAc-T$^{-/-}$* (n=5) mice compared to wild type (n=3), but only reached significance in *CST$^{-/-}$* nerve. C) Peripheral nerve MAG immunostaining was comparable among genotypes. Scale bar = 20 µm. Graphs display the means and ±SEM for each genotype,), and statistical analysis performed (one-way ANOVA followed by Tukey's *post-hoc* tests to compare multiple comparisons, indicated on the graphs as follows: *p<0.05; **p<0.01; ***p<0.001).

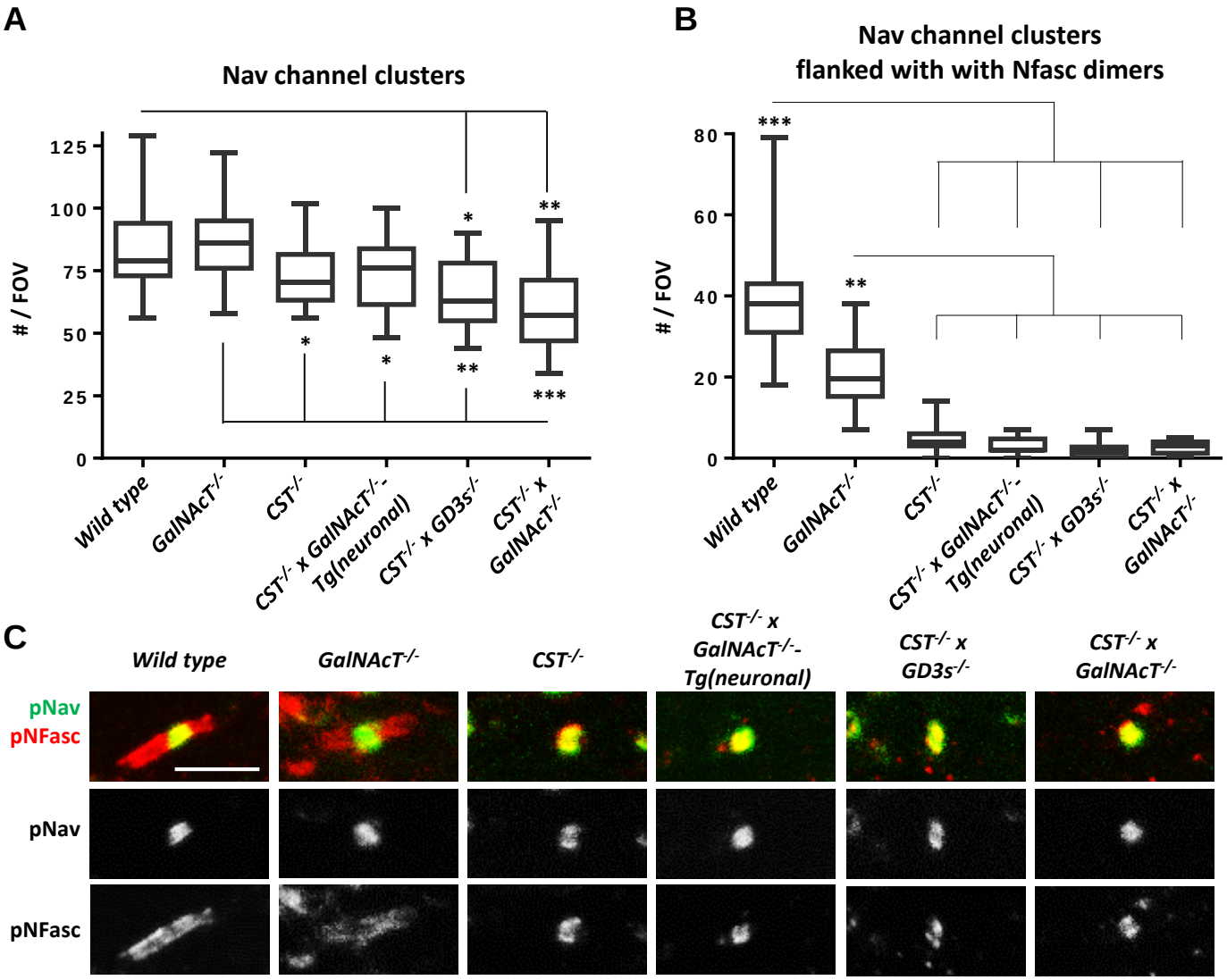

Figure 4. Loss of both sulfatide and complex gangliosides results in a modest reduction in CNS Nav channel cluster number and sulfatide deficiency reduces NF155 presence at parnodal loops. A) The number of Nav channel clusters significantly decreases in glycolipid deficient mouse optic nerves (n=3-4/genotype). Reintroducing a- and b-series gangliosides into neurons rescues this feature. B) Nav channel clusters flanked by normal paranodal neurofascin are significantly reduced in number when sulfatide is not expressed (n=2-3/genotype). Box-and whisker plots are used to display the spread of all data points collected from each animal then means were calculated per genotype for statistical analysis (one-way ANOVA followed by Tukey's *post-hoc* tests to compare multiple comparisons, indicated on the graphs as follows: *p<0.05; **p<0.01; ***p<0.001). C) Representative images of optic nerve sections from each genotype double-immunostained for pan-voltage gated sodium channel (pNav) antibody (green) and pan-neurofascin (pNFasc) antibody (red). Na channel clusters were observed in every genotype. pNFasc immunostaining formed a long band crossing the node and paranodes in WT and *GalNAc-T*$^{-/-}$ mice suggesting labelling of the NF186 and NF155 isoforms, respectively. All of the genotypes lacking sulfatide expression had pNFasc staining restricted to the node of Ranvier and co-localising only with pNav staining, suggesting presence of only the NF186 isoform of neurofascin. Scale bar = 5 µm.

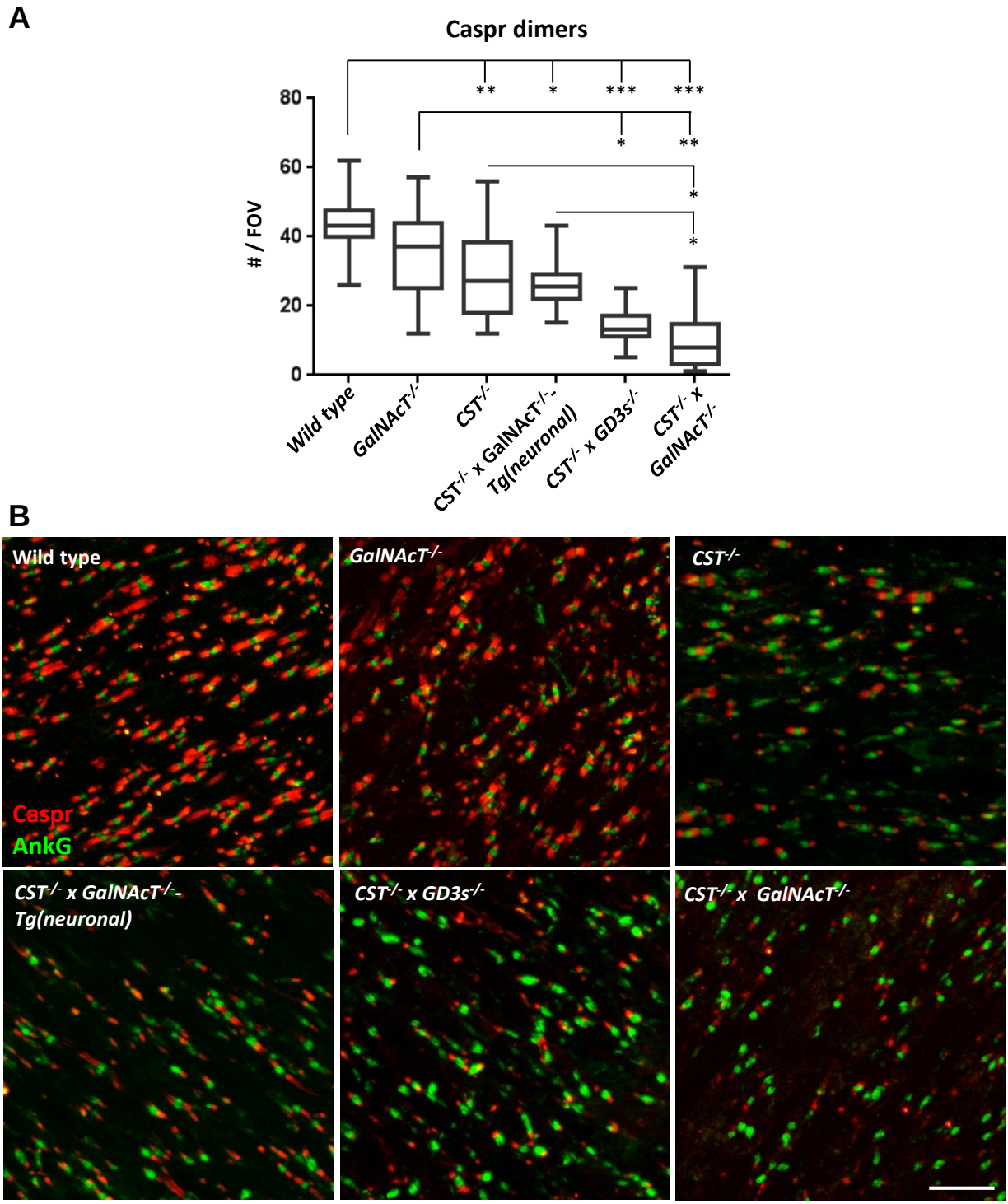

Figure 5. Paranodal Caspr dimer immunostaining in CNS tissue is progressively reduced with increasing glycolipid deficiency. A) *CST*$^{-/-}$ *x GalNAc-T*$^{-/-}$ and *CST*$^{-/-}$ *x GD3s*$^{-/-}$ mice have significantly fewer Caspr dimers per field of view (FOV) compared to WT and *GalNAc-T*$^{-/-}$ mice, and are not significantly different to each other (n=2-5/genotype). Caspr dimer number is improved to levels within *GalNAc-T*$^{-/-}$ mice range, but not WT, in *CST*$^{-/-}$ and *CST*$^{-/-}$ x *GalNAc-T*$^{-/-}$*-Tg(neuronal)* mice, which both display significantly more Caspr dimers than *CST*$^{-/-}$ *x GalNAc-T*$^{-/-}$ mice. Box-and whisker plots are used to display the spread of all data points collected from each animal then means were calculated per genotype for statistical analysis (one-way ANOVA followed by Tukey's *post-hoc* tests to compare multiple comparisons, indicated on the graphs as follows: *p<0.05; **p<0.01; ***p<0.001). B) Representative images of optic nerve sections from each genotype double-immunostained for Caspr (red) and nodal marker AnkyrinG (green) show the reduction in Caspr dimer number with diminishing glycolipid expression. Scale bar = 10 µm.

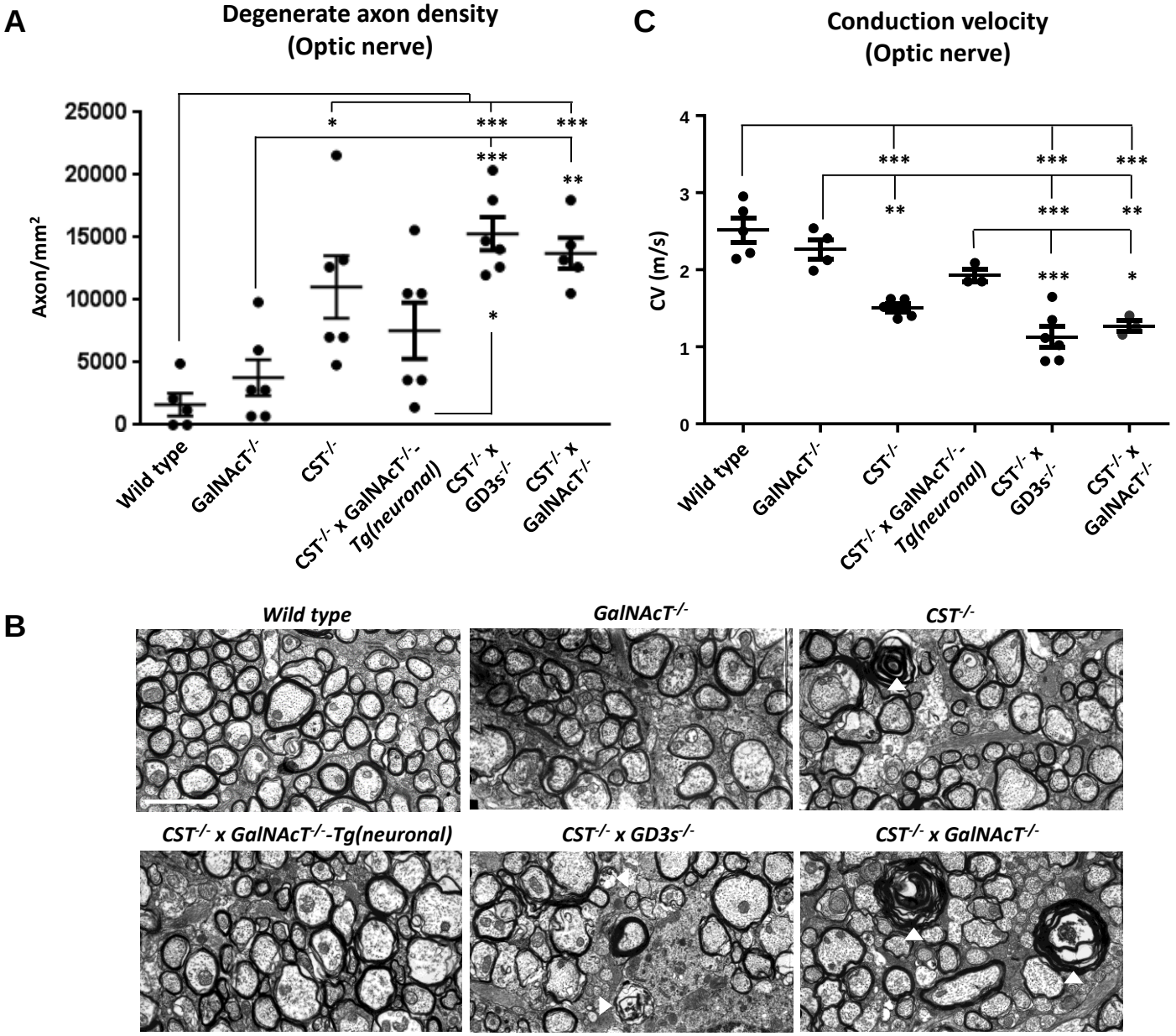

Figure 6. Glycolipid deficiency reduces CNS axon survival and function. A) Degenerate axon number increases to a significant level compared to wild type in optic nerves from *CST$^{-/-}$, CST$^{-/-}$ x GD3s$^{-/-}$* and *CST$^{-/-}$ x GalNAc-T$^{-/-}$* mice. Reintroducing a- and b-series gangliosides into neurons rescues this pathology. B) Electron micrographs depict the differences among the genotypes: white arrowheads indicate degenerate axons. Myelin is similar among mouse lines. C) A reduction in conduction velocity was observed in optic nerves from *CST$^{-/-}$, CST$^{-/-}$ x GD3s$^{-/-}$* and *CST$^{-/-}$ x GalNAc-T$^{-/-}$* mice. There was a reduction in conduction velocity in *CST$^{-/-}$ x GalNAc-T$^{-/-}$-Tg(neuronal)* mice, but this did not reach significance and was improved to within wild type and *GalNAc-T$^{-/-}$* rates. One-way ANOVA followed by Tukey's *post-hoc* tests to compare multiple comparisons, indicated on the graphs as follows: *p<0.05; **p<0.01; ***p<0.001. Scale bar = 2 µm.

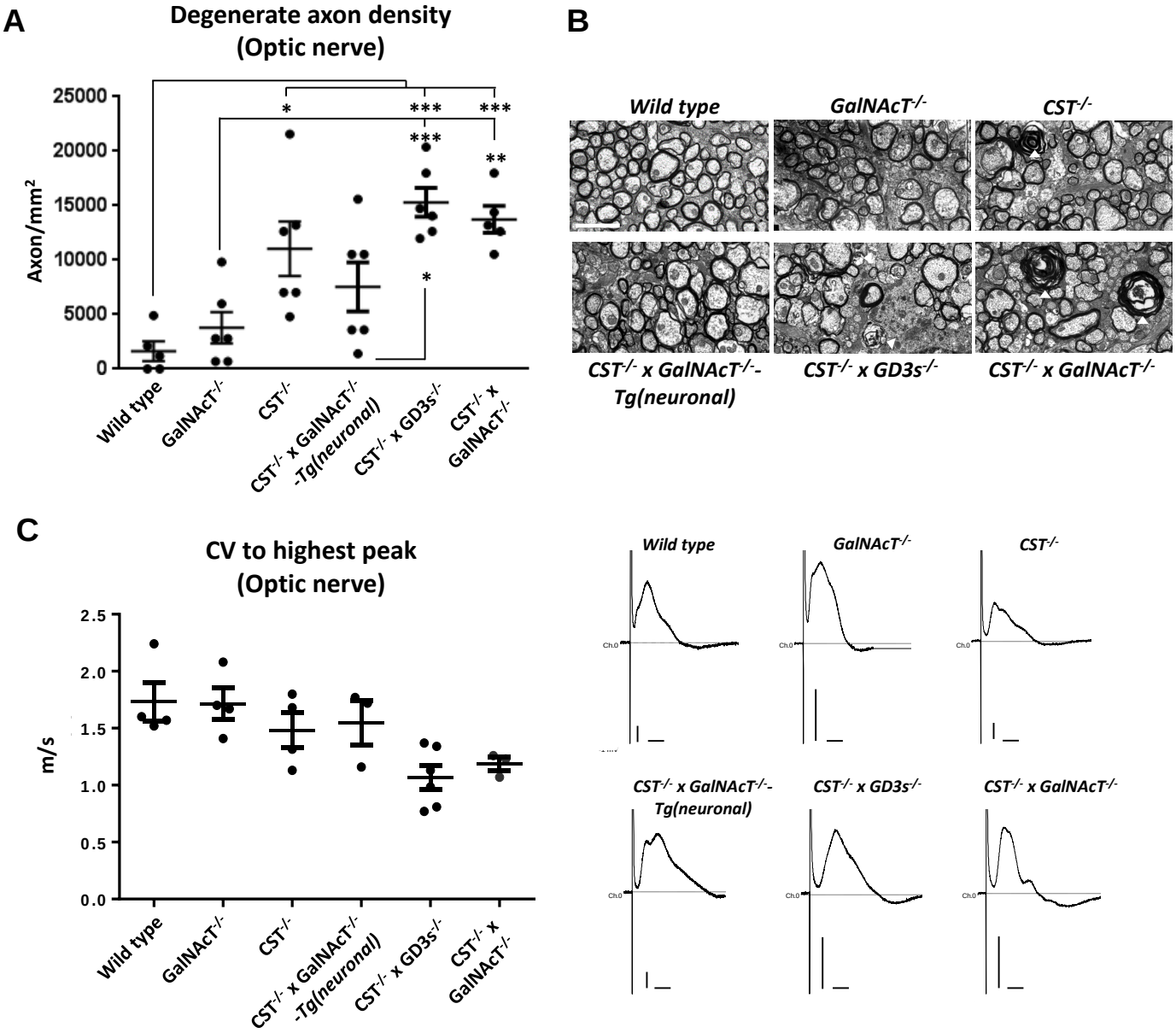

Figure 6. Glycolipid deficiency reduces CNS axon survival and function. A) Degenerate axon number increases to a significant level compared to wild type in optic nerves from *CST$^{-/-}$, CST$^{-/-}$ x GD3s$^{-/-}$* and *CST$^{-/-}$ x GalNAc-T$^{-/-}$* mice. Reintroducing a- and b-series gangliosides into neurons rescues this pathology. B) Electron micrographs depict the differences among the genotypes: white arrowheads indicate degenerate axons. Myelin is similar among mouse lines. Scale bar = 2 µm C) A reduction in conduction velocity was observed in optic nerves with diminishing glycolipid content. Representative CAP traces from each genotype show the normal waveform in WT, *GalNAc-T$^{-/-}$* and *CST$^{-/-}$ x GalNAc-T$^{-/-}$-Tg(neuronal)* optic nerves, however the waveform becomes abnormal in the *CST$^{-/-}$, CST$^{-/-}$ x GD3s$^{-/-}$* and *CST$^{-/-}$ x GalNAc-T$^{-/-}$* mice. One-way ANOVA followed by Tukey's *post-hoc* tests to compare multiple comparisons, indicated on the graphs as follows: *p<0.05; **p<0.01; ***p<0.001. Horizontal scale bar = 2 ms, vertical scale bar = 1 mV.

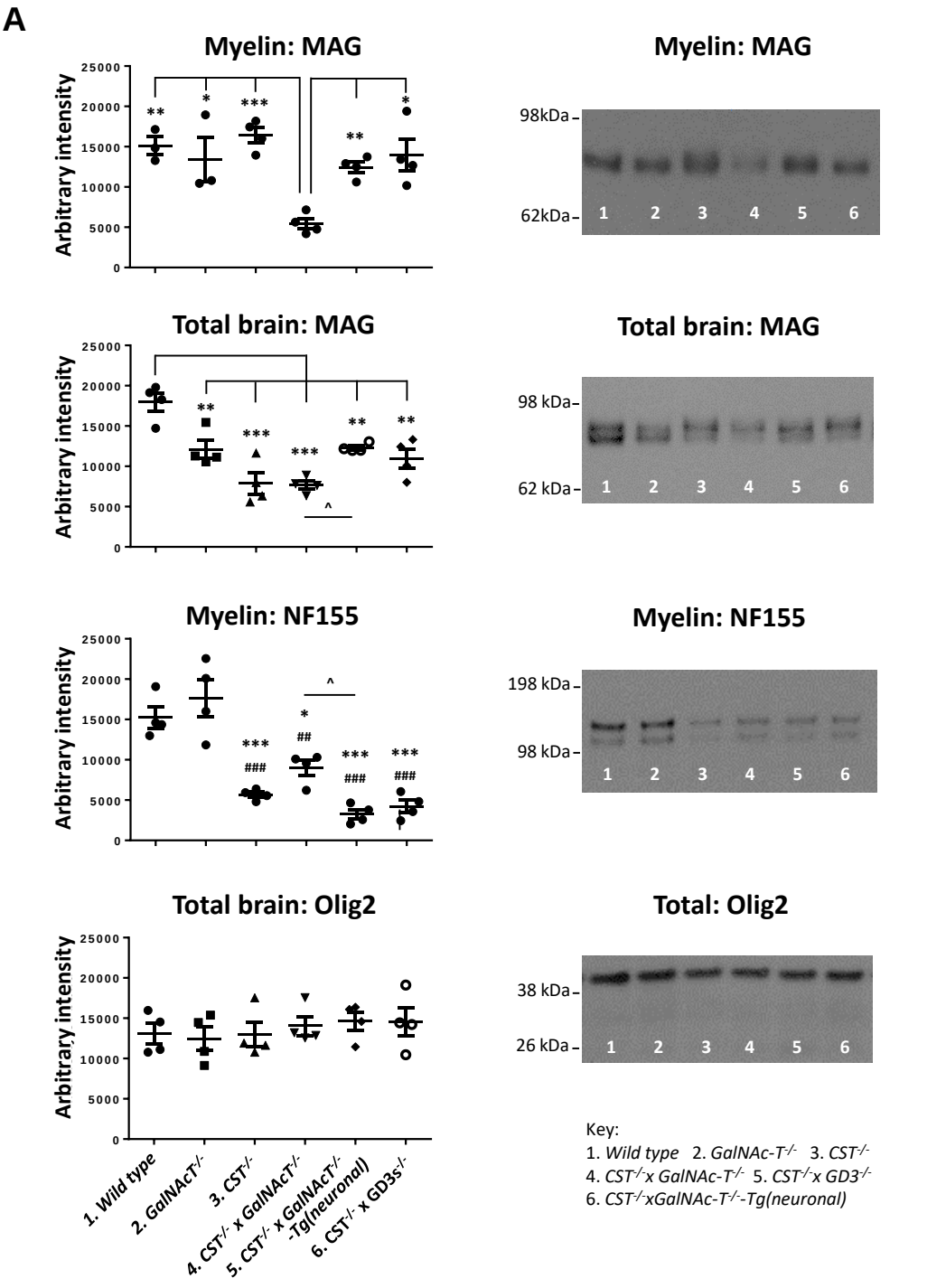

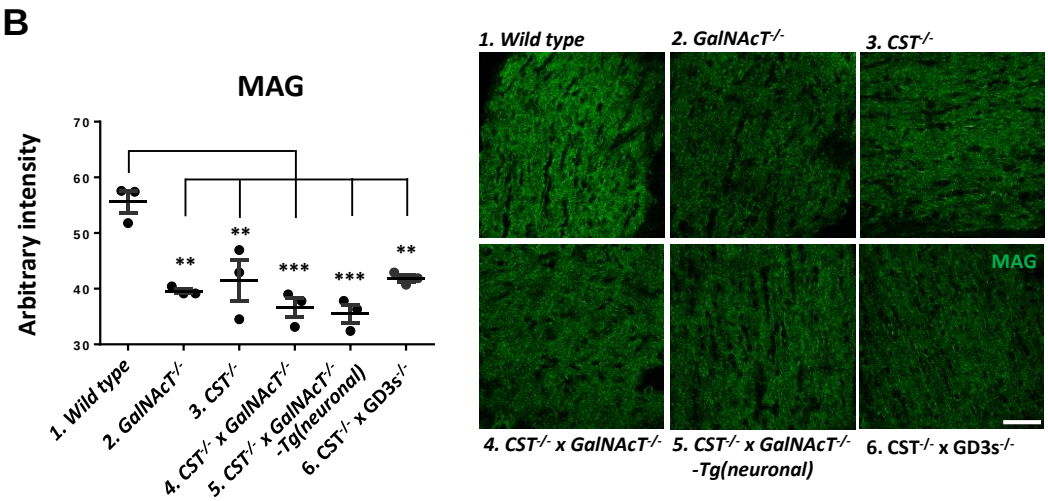

Figure 7. *N.B. New order of genotypes*. MAG and NF155 expression in the myelin fraction is altered by glycolipid deficiency. A) In the myelin fraction from P22 brain homogenates (n=4/genotype), MAG is significantly reduced in *CST$^{-/-}$ x GalNAc-T$^{-/-}$* mice compared to all genotypes, which do not significantly differ from one another (upper graph). All genotypes have a significant reduction in MAG expression in whole brain homogenate compared to WT (middle graph). Myelin NF155 was significantly reduced in all genotypes compared to WT (indicated by *) and *GalNAc-T$^{-/-}$* (indicated by #), which had similar levels (lower graph). ^indicates significant difference between *CST$^{-/-}$ x GalNAc-T$^{-/-}$* and *CST$^{-/-}$ x GalNAc-T$^{-/-}$-Tg(neuronal)* mice. Olig2 is unchanged by altered glycolipid expression. Representative blots show protein intensity per genotype, indicated by the corresponding number indicated in the key. B) P22 optic nerve MAG immunostaining (n=3/genotype) is significantly reduced in all genotypes compared to *wild type* nerve, which do not significantly differ from one another. Representative images show MAG immunostaining per genotype. Means were calculated per genotype for statistical analysis (one-way ANOVA followed by Tukey's *post-hoc* tests to compare multiple comparisons, indicated on the graphs as follows: *p<0.05; **p<0.01; ***p<0.001). Scale bar = 50 µm.

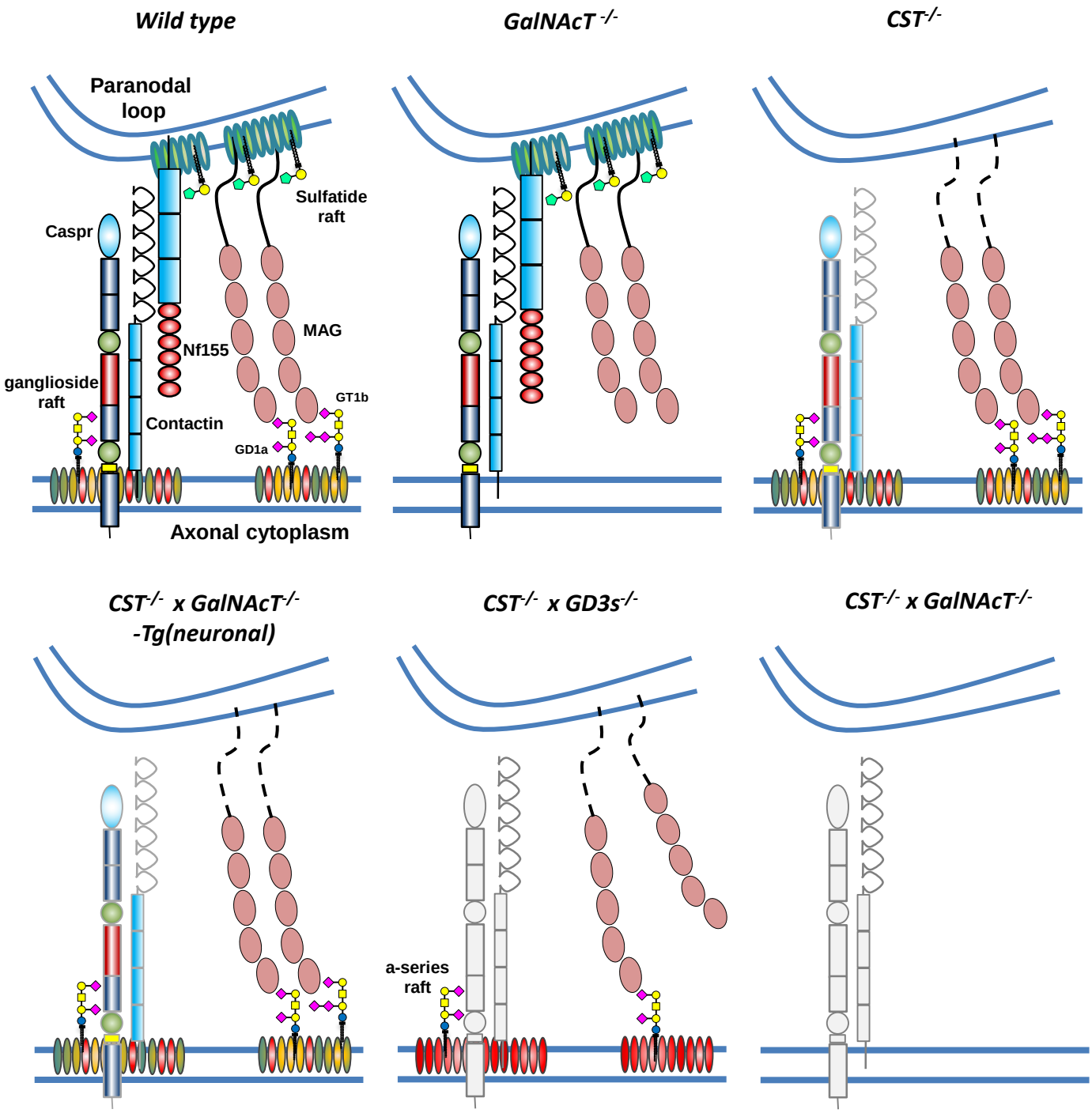

Figure 8. Schematic depicting the glycolipid rafts and changes to their associated paranodal proteins Caspr, NF155 and MAG composition in our transgenic mouse lines. GD1a and GT1b are represented in the ganglioside rafts as they are the major ligands of MAG, however, in reality the rafts would contain all complex gangliosides. Normally GD1a and GT1b in rafts will tether MAG but in their absence MAG does not make the axo-glial connection. If NF155 is present, this protein can partner with Caspr/Contactin to make an axo-glial junction. However, when sulfatide is absent, NF155 is also lost from the paranode. In the absence of NF155, Caspr presence is also diminished, especially with loss of complex ganglioside rafts. Under both ganglioside and sulfatide raft deficiency, we propose that MAG and NF155 are both absent from the paranodal axo-glial domain.